Article

Bifunctional Naphtho[2,3-d][1,2,3]triazole-4,9-dione Compounds Exhibit Antitumor Effects In Vitro and In Vivo by Inhibiting Dihydroorotate Dehydrogenase and Inducing Reactive Oxygen Species Production

zeping zuo, Xiaocong Liu, Xinying Qian, Ting Zeng, Na Sang, Huan Liu, Yue Zhou, Lei Tao, Xia Zhou, Na Su, Yamei Yu, Qiang Chen, Youfu Luo, and Ying-Lan Zhao

Just Accepted

1
2
3
4
5
6
7
8
9
10
11
12
13
14
15
16
17
18
19
20
21
22
23
24
25
26
27
28
29
30
31
32
33
34
35
36
37
38
39
40
41
42
43
44
45
46
47
48
49
50
51
52
53
54
55
56
57
58
59
60

Bifunctional Naphtho[2,3-*d*][1,2,3]triazole-4,9-dione Compounds Exhibit Antitumor Effects *In Vitro* and *In Vivo* by Inhibiting Dihydroorotate Dehydrogenase and Inducing Reactive Oxygen Species Production

Zeping Zuo,[a,#] Xiaocong Liu,[a,#] Xinying Qian,[a,#] Ting Zeng,[a,#] Na Sang,[a] Huan Liu,[a] Yue Zhou,[a] Lei Tao,[a] Xia Zhou,[a] Na Su,[c] Yamei Yu,[a] Qiang Chen,[a] Youfu Luo,[a,*] Yinglan Zhao[a,b,*]

[a] State Key Laboratory of Biotherapy and Cancer Center, West China Hospital, West China Medical School, Sichuan University, and Collaborative Innovation Center for Biotherapy, Chengdu, 610041, China

[b] West China School of Pharmacy, Sichuan University, Chengdu, 610041, China

[c] Department of Pharmacy, West China Hospital, Sichuan University, Chengdu 610041, China.

ABSTRACT

Human dihydroorotate dehydrogenase (*h*DHODH) is an attractive target for cancer therapy. Based on its crystal structure, we designed and synthesized a focused compound library containing the structural moiety of 1,4-benzoquinone which possesses reactive oxygen species (ROS) induction capacity. Compound **3s** with a naphtho[2,3-*d*][1,2,3]triazole-4,9-dione scaffold exhibited inhibitory activity against *h*DHODH. Further optimization led to compounds **11k** and **11l** which inhibited *h*DHODH activity with IC$_{50}$ values of 9 nM and 4.5 nM, respectively. Protein-ligand cocrystal structures clearly depicted hydrogen bond and hydrophobic interactions of **11k** and **11l** with *h*DHODH. Compounds **11k** and **11l** significantly inhibited leukemia cells and solid tumor cells proliferation, induced ROS production, mitochondrial dysfunction, apoptosis and cell cycle arrest. Nanocrystallization of compound **11l** displayed significant *in vivo* antitumor effects in Raji xenograft model. Overall, this study provides a novel bifunctional compound **11l** with *h*DHODH inhibition and ROS induction efficacy which represents a promising anticancer lead worth further

INTRODUCTION

Human dihydroorotate dehydrogenase (*h*DHODH) is the fourth and rate-limiting enzyme in the pyrimidine *de novo* synthesis pathway, which is located in the inner mitochondrial membrane[1,2]. In addition to catalyzing the oxidation of dihydroorotate to orotate with the participation of the cofactors flavin mononucleotide (FMN) and ubiquinone, *h*DHODH reduces ubiquinone, linking the pyrimidine pathway to the mitochondrial respiratory chain[3]. Overexpression of *h*DHODH has been observed in many cancers, including acute myeloid leukemia (AML)[4,5], colorectal cancer, melanoma and pancreatic cancer, and is negatively associated with the poor survival rate of cancer patients[6–9]. Knockdown of *h*DHODH effectively inhibits cancer cell proliferation, invasion and migration. The inhibition of *h*DHODH is a strategy for overcoming the differentiation blockade in AML, and affects ATP depletion, endogenous ROS and the mediation of S-phase arrest in cancer cells[10]. Additionally, *h*DHODH inhibitors sensitize multiple cancers to chemotherapy. Triple-negative breast cancer cells exhibited reduced chemotherapy resistance and were sensitized to genotoxic chemotherapy agents after *h*DHODH inhibition[11]. Hence, *h*DHODH is a promising target with a vital role in the treatment of cancers.

Leflunomide and brequinar (BRQ) are two representative *h*DHODH inhibitors (Figure 1A). Leflunomide, an FDA-approved drug for the treatment of rheumatoid arthritis and psoriatic arthritis, was the first reported *h*DHODH inhibitor[12,13]. The second reported *h*DHODH inhibitor, BRQ, was initially applied in therapy to prevent organ transplant rejection and then regarded as an antitumor agent for multiple cancer treatments[14,15]. The antitumor efficiency of leflunomide and BRQ was evaluated in clinical trials against several malignancies, including melanoma and breast cancer. However, no approval was obtained for their clinical use in cancer treatment because of their limited efficiency and potential toxicity[16–21]. More recently, an increasing number of new *h*DHODH inhibitors have been investigated for cancer treatment[22,23]. 4-Quinoline carboxylic acids and 2-hydroxypyrazolo[1,5-a]pyridine *h*DHDOH inhibitors

were investigated for the treatment of colorectal cancer and AML in preclinical studies [24,25]. ASLAN003[26], BAY2402234[27] and AG-636[28] were explored to treat AML in Phase II clinical trials in 2017, leukemia in Phase I clinical trials in 2018 and lymphoma in Phase I clinical trials in 2019, respectively (Figure 1A). BAY2402234 showed strong anti-myeloid malignancies with good ADME properties[29]. However, all of the above-mentioned hDHODH inhibitors have not yet achieved success as a marketed drug to clinically treat cancers. Consequently, the discovery of diverse classes of hDHODH inhibitors with beneficial properties is desirable.

Emerging studies have suggested that hDHODH depletion partially inhibits the respiratory chain complex III, decreases the mitochondrial membrane potential, and increases reactive oxygen species (ROS) generation[30]. ROS are chemically reactive molecules that have essential functions in living organisms. Excessive amounts of ROS cause oxidative damage to the lipids, proteins and DNA of cancer cells[31]. ROS induction leads to the preferential killing and selective eradication of cancer cells[32]. Therefore, manipulating ROS levels by redox modulation is a way to selectively kill cancer cells. Pharmacological use of ROS-inducing small molecules is considered an effective strategy to combat against cancer.

It has been confirmed that compounds with a benzoquinone moiety can induce ROS and apoptosis in cells. As shown in Figure 1B, the structural moiety of benzoquinone is found to be included in many marketed anticancer drugs and investigational agents[33–37]. Interestingly, ubiquinone derivatives are found to exhibit inhibitory activity against hDHODH. For example, decylubiquinone binds to the putative ubiquinone binding pocket of hDHODH. DCL[38], another ubiquinone derivative, could interrupt the oxidation of dihydroorotate with an IC_{50} value of 67 nM against hDHODH. Moreover, atovaquone, an antimalarial drug with a modest inhibitory effect against $P.$ $falciparum$ DHODH (PfDHODH) in $vitro$ (K_i = 27 μM) and weak inhibitory effect against hDHODH (IC_{50} = 14.5 μM) contains benzoquinone fragments[38,39]. Thus, the compounds with the structural moiety of benzoquinone might inhibit the activity of hDHODH and induce the production of ROS.
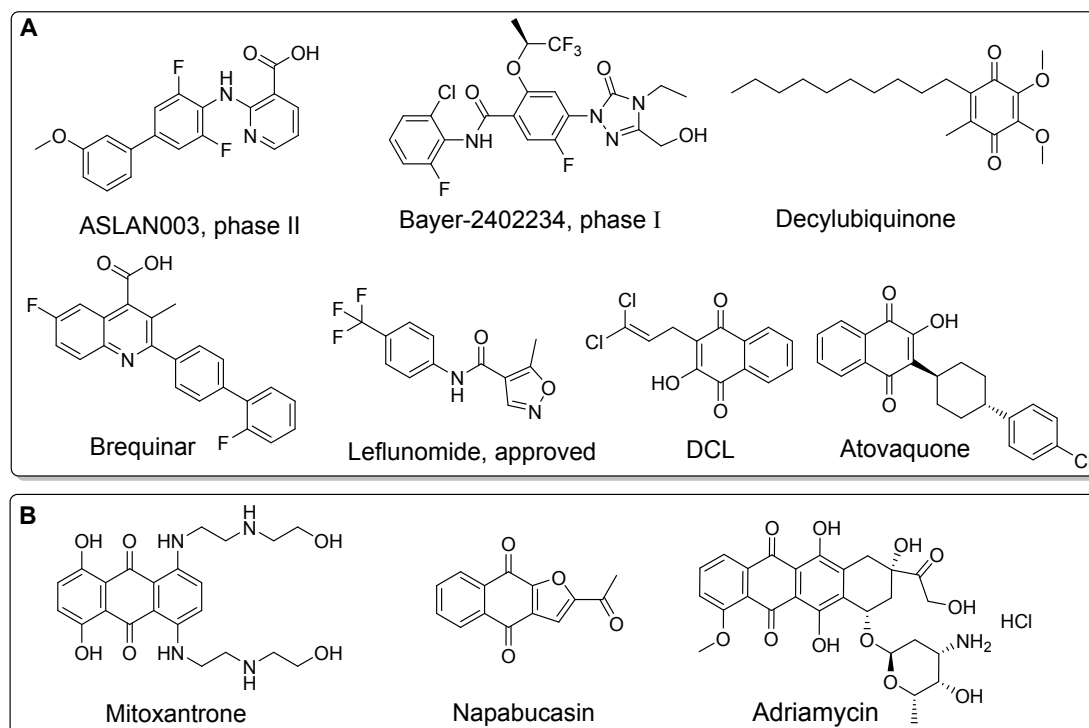
Figure 1. Chemical structures of reported *h*DHODH inhibitors and anticancer agents with benzoquinone moiety. (A) Selected *h*DHODH inhibitors. (B) Anticancer agents with ROS induction capability.

Based on the observations described above and the crystal structure of *h*DHDOH, we designed a focused library of compounds containing the structural moiety of 1, 4-benzoquinone to obtain active compounds with *h*DHODH inhibition and ROS-inducing effects. In glide-docking experiments, we found that compounds with a naphtho[2,3-*d*][1,2,3]triazole-4,9-dione scaffold possessed favorable binding mode to the protein target (Figure 2A). The compound with a phenyl group substituted at the *N*-1 position of the triazole ring occupied the proposed putative ubiquinone tunnel in *h*DHODH (PDB ID: 1D3G). Notably, it formed hydrogen bonds with the amino acid residues R136 and Q47, which is similar to decylubiquinone (Figure 2B) and DCL (Figure 2C). Furthermore, additional hydrophobic interactions were observed between the *N*-1 phenyl group of the described molecules and *h*DHODH. Thus, it is plausible that the described molecules with hydrophobic substituents in the *N*-1 position of the triazole ring may be bound to *h*DHODH and are promising agents for *h*DHODH inhibition.
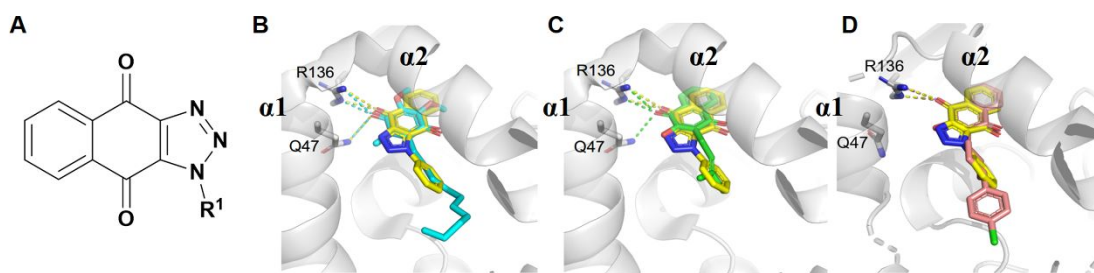
Figure 2. Chemical structures of designed *h*DHODH inhibitors and docking models with *h*DHODH. (A) The designed naphtho[2,3-*d*][1,2,3]triazole-4,9-dione compound. (B) Docking models of a typical naphtho[2,3-*d*][1,2,3]triazole-4,9-dione compound (yellow) and decylubiquinone (cyan) with *h*DHODH. (C) Docking models of a typical naphtho[2,3-*d*][1,2,3]triazole-4,9-dione compound (yellow) and DCL (green) with *h*DHODH. Hydrogen bonds are shown as dashed lines. (D) Docking models of a typical naphtho[2,3-*d*][1,2,3]triazole-4,9-dione compound (yellow) and atovaquone (pink) with *h*DHODH. Hydrogen bonds are shown as dashed lines.

In the present study, we describe the design, synthesis, structure–activity relationship (SAR) investigation, and X-ray crystallographic analysis of novel bifunctional anticancer agents. The *in vitro* and *in vivo* biological assays (including cell proliferation, cell cycle, apoptosis, uridine supplementation rescue experiment, pharmacokinetics study, xenograft experiment and acute toxicity evaluation) were performed to characterize the biological effects and action mechanisms of the designed molecules. Our finding provides a novel structural class of *h*DHODH inhibitors with ROS induction capability for cancer treatment.

RESULTS AND DISCUSSION

2.1 Chemistry

To quickly access a panel of naphtho[2,3-*d*][1,2,3]triazole-4,9-dione compounds for evaluating *h*DHODH inhibition, aryl azide building blocks with diverse structural features were synthesized. As illustrated in synthetic route A[40], the aryl azide intermediates **2a**–**t** were prepared from aryl boronic acids or aryl borates under copper-catalyzed conditions. The final naphtho[2,3-*d*][1,2,3]triazole-4,9-dione compounds **3a**–**t** were made by condensation 2-hydroxynaphthalene-1,4-dione with different aryl azides from the previous step. The Suzuki reaction was mainly employed to synthesize

biphenyl azides with various substituent groups on either phenyl ring, which enabled us to perform a more extensive SAR study (routes B and C)[41, 42]. Routes B and C differ principally by the occurrence of such Suzuki couplings with a reactive functional group R_2 (-OH, -NH$_2$) generated at a late and early stage, respectively. The advantage of route B is that R_2 groups with sensitive moieties can be successfully added to produce biphenyl azides in high yields. However, route C was less tolerant of such hydrophilic moieties and unable to obtain the desired compounds in a satisfactory manner. To expand our SAR beyond the naphtho[2,3-*d*][1,2,3]triazole-4,9-dione limitations, we developed routes D and E. Route D introduced diversity through the different substituent 2-hydroxy naphthalene-1,4-dione via oxidation reaction with suitable precursors, and route E enabled diversity through classic click chemistry between different alkynyl and aryl azides. Double bond reduction was carried out by sodium hydride to yield the corresponding alcohol (**14j**). From routes B–E, we obtained compounds **7a–g**, **11a–s**, **14a–l**, and **14k–l**, respectively.

Scheme 1. Synthesis of Naphtho[2,3-*d*][1,2,3]Triazole-4,9-Dione Analogs

Synthetic route A
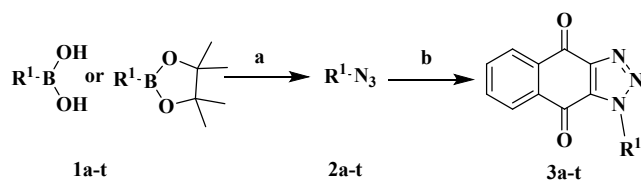
1a, 2a, 3a : R^1 = 2-cyanophenyl	**1k, 2k, 3k : R^1 =** 6-chloropyridin-3-yl
1b, 2b, 3b : R^1 = 3-nitrilephenyl	**1l, 2l, 3l : R^1 =** 2-chloropyridin-4-yl
1c, 2c, 3c : R^1 = 3-hydroxyphenyl	**1m, 2m, 3m : R^1 =** pyridin-4-yl
1d, 2d, 3d : R^1 = 2-methoxyphenyl	**1n, 2n, 3n : R^1 =** naphthalen-2-yl
1e, 2e, 3e : R^1 = 3-iodophenyl	**1o, 2o, 3o : R^1 =** 2*H*-1,3-benzodioxol-5-yl
1f, 2f, 3f : R^1 = 3-aminophenyl	**1p, 2p, 3p : R^1 =** 1*H*-1,3-benzodiazol-2-yl
1g, 2g, 3g : R^1 = 4-isopropylphenyl	**1q, 2q, 3q : R^1 =** 4-(pyridin-3-yl)phenyl
1h, 2h, 3h : R^1 = 2-(trifluoromethyl)phenyl	**1r, 2r, 3r : R^1 =** 4-(pyridin-4-yl)phenyl
1i, 2i, 3i : R^1 = 4-fluoro-3-methylphenyl	**1s, 2s, 3s : R^1 =** 1,1'-biphenyl]-4-yl
1j, 2j, 3j : R^1 = 4-methyl-3-(trifluoromethyl)phenyl	**1t, 2t, 3t : R^1 =** 6-(morpholin-4-yl)pyridin-3-yl

Reagents and conditions. (a) Aryl boronic acid or borate, NaN$_3$, CuSO$_4$, MeOH, 80 °C, overnight (45–78%). (b) 2-Hydroxynaphthalene-1,4-dione, DBU, CH$_3$CN, 80 °C, 3–4 h (34–64%).
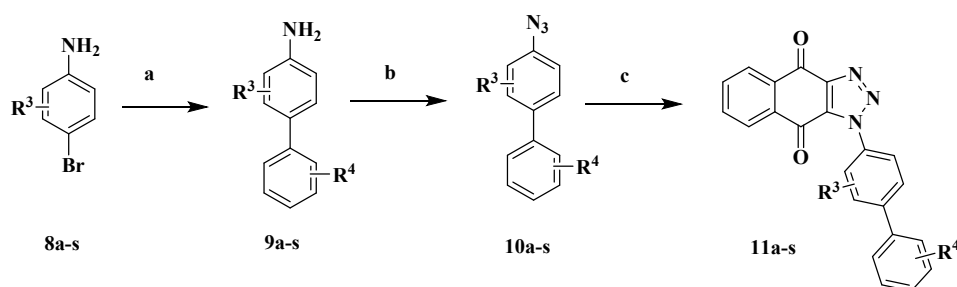
Synthetic route B
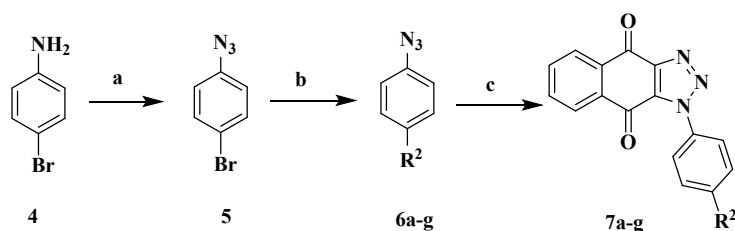
6a, 7a : R^2 = pyrimidin-5-yl

6b, 7b : R^2 = 2-methylpyridin-4-yl

6c, 7c : R^2 = 2-hydroxyphenyl-1-yl

6d, 7d : R^2 = 3-hydroxyphenyl-1-yl

6e, 7e : R^2 = 4-aminophenyl-1-yl

6f, 7f : R^2 = 3-aminophenyl-1-yl
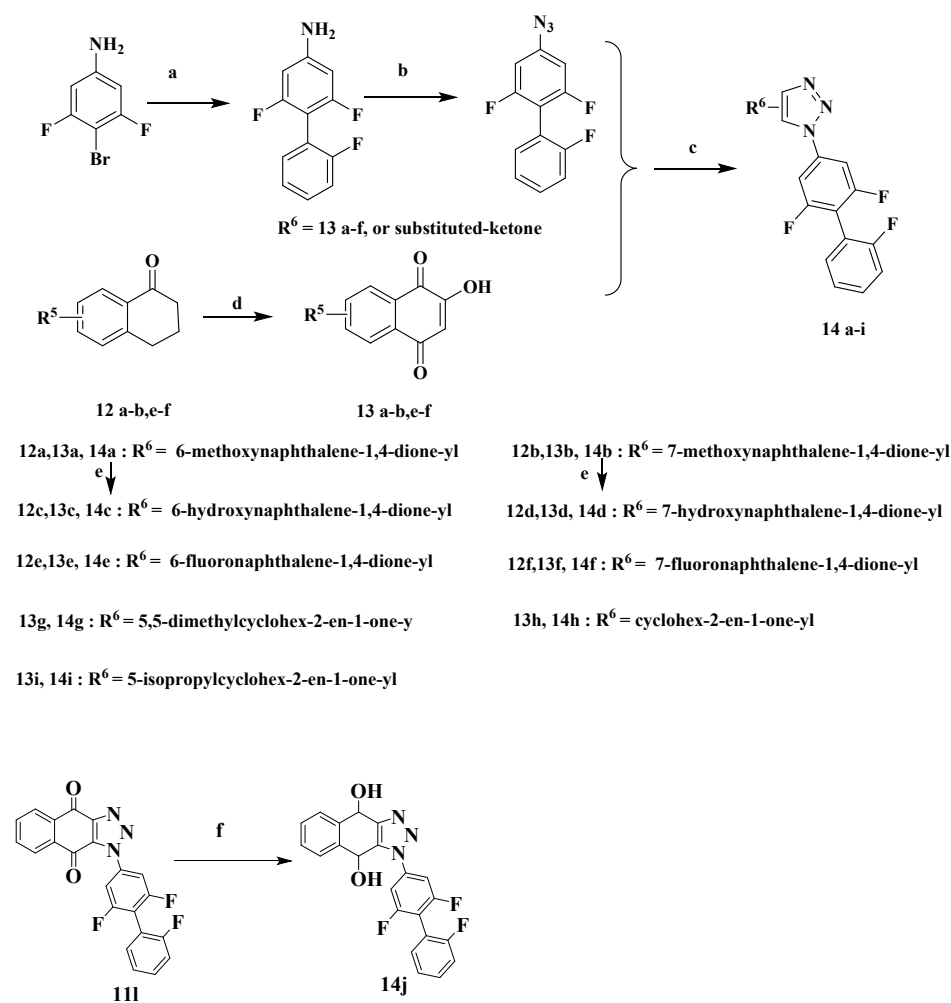
6g, 7g : R^2 = 2-aminophenyl-1-yl

Reagents and conditions. (a) (i) Tert-butylnitrite, THF, -20 °C to rt, 2 h. (ii) NaN$_3$, CH$_3$CN/H$_2$O (30–79%). (b) Aryl boronic acid or borate, Pd(dppf)Cl$_2$·DCM, Cs$_2$CO$_3$ or K$_2$CO$_3$, 1,4-dioxane/H$_2$O, overnight (30–75%). (c) 2-Hydroxynaphthalene-1,4-dione, DBU, CH$_3$CN, 80 °C, 3–4 h (34–64%).

Synthetic route C

9a, 10a, 11a : R^3= H, R^4=2'-F

9b, 10b, 11b : R^3 = H, R^4 =3'-F

9c, 10c, 11c : R^3 = H, R^4 =3'-COOCH$_3$

9d, 10d, 11d : R^3 = H, R^4 =3', 4', 5'-OCH$_3$

9e, 10e, 11e : R^3 = 2-OCH$_3$, R^4 = H

9f, 10f, 11f : R^3= H, R^4= 3'-OCH$_3$

9g, 10g, 11g : R^3 = H, R^4 = 3', 5'-bis(trifluoromethyl)

9h, 10h, 11h : R^3 = 3-F, R^4 = 4'-isopropyl

9i, 10i, 11i : R^3 = 3, 5-difluoro, R^4 = 4'-isopropyl

9j, 10j, 11j : R^3= 2, 6-difluoro, R^4= 4'-isopropyl

9k, 10k, 11k : R^3 = 2, 6-difluoro, R^4 = 3'-OCH$_3$

9l, 10l, 11l : R^3 = 2, 6-difluoro, R^4 = 2'-F

9m, 10m, 11m : R^3= 2, 6-difluoro, R^4 = 3'-F

9n, 10n, 11n : R^3 = 2, 6-difluoro, R^4 = 4'-F

9o, 10o, 11o : R^3 = 2, 6-difluoro, R^4 = 3'-CH$_2$OH

9p, 10p, 11p : R^3 = 2, 6-difluoro, R^4 = 3'-CH$_2$OCH$_3$

9q, 10q, 11q : R^3 = 2, 6-difluoro, R^4 = 3'-CH$_2$COOCH$_3$

9r, 10r, 11r : R^3= 2, 6-difluoro, R^4 = 3'-N(CH$_3$)$_2$

9s, 10s, 11s : R^3 = 2, 6-difluoro, R^4 = 2'-F, 3'-CH$_2$OH

Reagents and conditions. (a) Aryl boronic acid or borate, Pd(dppf)Cl$_2$·DCM, Cs$_2$CO$_3$ or K$_2$CO$_3$, 1,4-dioxane/H$_2$O, 100 °C, overnight (30–75%). (b) (*i*) Boron trifluoride diethyl etherate, *Tert*-butylnitrite, THF, -20 °C to rt, 2 h. (*ii*) NaN$_3$, CH$_3$CN/H$_2$O (30–79%). (c) 2-Hydroxynaphthalene-1,4-dione, DBU, CH$_3$CN, 80 °C, 3–4 h (34–64%).

Synthetic route D

R⁶ = 13 a-f, or substituted-ketone

12 a-b,e-f   **13 a-b,e-f**

14 a-i

12a,13a, 14a : R⁶ = 6-methoxynaphthalene-1,4-dione-yl   **12b,13b, 14b : R⁶ = 7-methoxynaphthalene-1,4-dione-yl**

12c,13c, 14c : R⁶ = 6-hydroxynaphthalene-1,4-dione-yl   **12d,13d, 14d : R⁶ = 7-hydroxynaphthalene-1,4-dione-yl**

12e,13e, 14e : R⁶ = 6-fluoronaphthalene-1,4-dione-yl   **12f,13f, 14f : R⁶ = 7-fluoronaphthalene-1,4-dione-yl**

13g, 14g : R⁶ = 5,5-dimethylcyclohex-2-en-1-one-y   **13h, 14h : R⁶ = cyclohex-2-en-1-one-yl**

13i, 14i : R⁶ = 5-isopropylcyclohex-2-en-1-one-yl

1l   **14j**

Reagents and conditions. (a) Boronic acid or boronic acid ester, Pd(dppf)Cl₂·DCM, Cs₂CO₃/K₂CO₃, 1,4-dioxane/H₂O, 100 °C, overnight (30–75%). (b) (*i*) Boron trifluoride diethyl etherate, *Tert*-Butylnitrite, THF, -20 °C to rt, 2 h, (*ii*) NaN₃, CH₃CN/H₂O (30–79%). (c) 2-Hydroxynaphthalene-1,4-dione, DBU, CH₃CN, 80 °C, 3–4 h (34–64%). (d) Anhydrous tert-butanol, O₂, Potassium tert-butoxide, 3 h, rt, 52-68%. (e) Boron tribromide, DCM, 0–5 °C, 64-67%. (f) Sodium hydride, MeOH, rt, 39%.

Synthetic route E
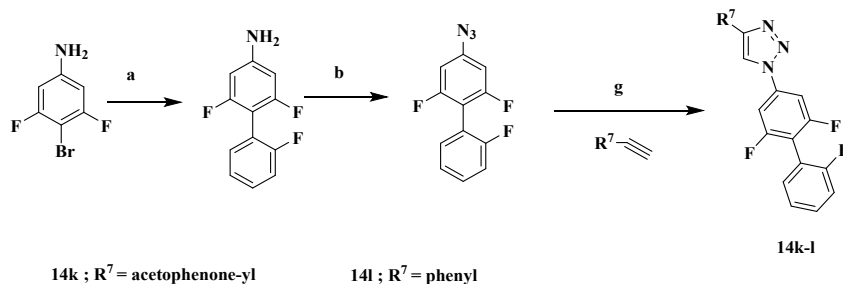
14k ; R⁷ = acetophenone-yl   14l ; R⁷ = phenyl

Reagents and conditions. (a) Boronic acid or boronic acid ester, Pd(dppf)Cl$_2$·DCM, Cs$_2$CO$_3$/K$_2$CO$_3$, 1,4-dioxane/H$_2$O, 100 °C, overnight (30–75%). (b) (i) Boron trifluoride diethyl etherate, *Tert*-Butylnitrite, THF, -20 °C to rt, 2 h. (ii) NaN$_3$, CH$_3$CN/H$_2$O (30–79%). (g) CuSO4 (0.02eq.), (+)-sodium L-ascorbate (0.1 eq) in 1:1 H$_2$O:t-BuOH, rt for 24 h 46% or 41%.
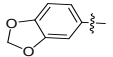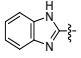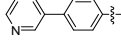
2.2 Structure-Activity Relationship (SAR)
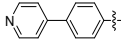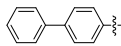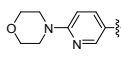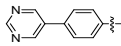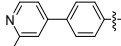
After visualization by *in silico* docking results, we firstly investigated the *h*DHODH inhibition activity of twenty naphtho[2,3-*d*][1,2,3]triazole-4,9-dione compounds with diverse *N*-1 substitutions of phenyl, pyridyl, naphthyl, benzimidazolyl and biaryl structures (Scheme 1A). Lipophilic ligand efficiency (LipE) is believed to be an important metric for prediction of absorption, distribution, metabolism, and excretion (ADME) properties and BRQ is a lipophilic drug that has relatively low LipE. Thus, in our medicinal chemistry campaign for finding novel *h*DHODH inhibitors as potential anticancer agents against solid tumors, we hope to modulate the LipE values of the compounds, while maintaining their *h*DHODH inhibitory effect. The results showed that compound **3s** with a diphenyl group at the *N*-1 position was the most potent for *h*DHODH inhibition (IC$_{50}$ = 19 nM), and it possessed an improved lipophilic ligand efficiency (LipE = 2.69) compared with BRQ (1.9). Compound **3q** with a 4-(4-(pyridin-3-yl)phenyl)-group at the *N*-1 position of the naphtho[2,3-*d*][1,2,3]triazole-4,9-dione scaffold had a better LipE value than compound **3s**, but exhibited a decreased activity against *h*DHODH with IC$_{50}$ value of 422 nM. Compound **3g** showed an enzyme inhibition (IC$_{50}$ = 560 nM) that was similar to compound **3q**, but had a lower LipE value than BRQ. Other compounds in this series did not exhibit inhibition more than 50% against *h*DHODH activity at maximum test concentration (1000 nM). Collectively,

these results indicated that compound with a diphenyl group at the *N*-1 position favors

*h*DHODH activity and improves lipophilic ligand efficiency, thus is worthy of further

optimization.

Table 1. Physicochemical Properties and Biological Activity of Compounds 3a–t and 7a–b
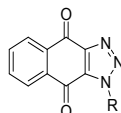
Compd	R	clogP	LipE	IC$_{50}$ (nM)
BRQ		6.38	1.9	5.2
3a		2.72	<3.28	>1000
3b		2.72	<3.28	>1000
3c		2.89	<3.11	>1000
3d		3.25	<2.75	>1000
3e		4.27	<1.73	>1000
3f		2.30	<3.70	>1000
3g		4.57	1.68	560
3h		4.03	<1.97	>1000
3i		3.79	<2.11	>1000
3j		4.53	<1.47	>1000
3k		2.77	<3.23	>1000
3l		2.77	<3.23	>1000
3m		2.05	<3.95	>1000
3n		4.32	<1.68	>1000

3o		3.20	<2.80	>1000
3p		2.99	<2.01	>1000
3q		3.54	2.83	422
3r		3.54	<2.46	>1000
3s		5.03	2.69	19
3t		2.05	<3.95	>1000
7a		2.38	<3.62	>1000
7b		4.03	<1.97	>1000
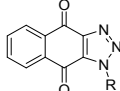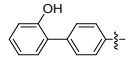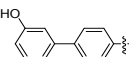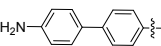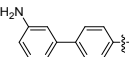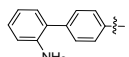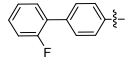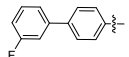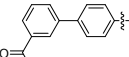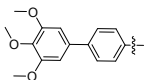
Data for cLogP values were predicted using ChemBioDraw Professional 14 Software. LipE was calculated as follows: LipE = -pIC$_{50}$ (M) -cLogP[43].

Considering compound **3s** with diphenyl skeleton exhibited potent inhibitory activity against *h*DHODH and improved LipE value, we next designed and synthesized twenty-four analogs by introducing diverse substituent groups at different positions of the diphenyl skeleton to further enhance the enzyme activity of compounds. As shown in Table 2, 50% of the synthesized analogs (12 out of 24) reached single-digit nanomolar IC$_{50}$ values. Four compounds (**11d**, **11g**, **11h** and **11i**) displayed low inhibitory effects with IC$_{50}$ values over 1000 nM. These compounds seemed to have substituent(s) that created high steric hindrances, such as the 3',4',5'-trimethoxy groups linked to compound **11d**, 3',5'-trifluoromethyl groups to **11g** and 4'-isopropyl groups to **11h** and **11i**. Nevertheless, compound **11j,** similarly bearing a 4'-isopropyl group, showed potent activity with an IC$_{50}$ value of 76 nM**,** which is much stronger than that of compound **11i**. The difference between compounds **11i** and **11j** is the location of two fluorine atoms. Compound **11i** is 2,6-difluorosubstitution, whereas compound **11j** is 3,5-difluorosubstitution. The helices α1 and α2 in *h*DHODH form a slot in the so-called hydrophobic patch, which narrows toward the proximal redox site (Figures 2B and 2C). The size of the tunnel and substituent may afford undesirable clashes or limit the degrees of conformational freedom. Compound **11i** with 3,5-difluorosubstitution might

results in a repulsive interaction with the hydrophobic patch, afford undesirable clashes or limit the degrees of conformational freedom, whereas compound **11j** with 2,6-difluorosubstitution might not. Thus, 2,6-difluorosubstitution is favored for enzyme inhibition activity over 3,5-difluorosubstitution. This observation prompted us to synthesize more analogs (**11k–s**) with the favored 2, 6-difluorosubstitution. All of these newly synthesized molecules displayed good inhibitory activity against *h*DHODH at nanomolar or subnanomolar concentrations (Table 2). Similar to lead compound **3s**, most of the active compounds described herein have improved lipE values, except for compound **11j**. The hydrophobic property of the propyl group on compound **11j** may account for its low lipE value (0.37).

Table 2. Physicochemical Properties and Biological Activity of Compounds 7c–g and 11a–s

Compd	R	clogP	LipE	IC_{50} (nM)
BRQ		6.38	1.9	5.2
7c		4.06	2.58	230
7d		4.36	3.32	21
7e		3.80	3.80	25
7f		3.80	4.7	3.1
7g		3.80	3.89	20
11a		5.17	3.17	4.5
11b		5.17	2.08	56
11c		5.00	1.26	550
11d		4.33	<1.67	>1000
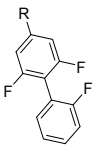
11e		4.58	3.80	4.1
11f		4.95	2.05	100
11g		6.80	<-0.8	>1000
11h		6.60	<-0.60	>1000
11i		6.75	<-0.75	>1000
11j		6.75	0.37	76
11k		5.24	2.8	9.0
11l		5.46	2.88	4.5
11m		5.46	3.10	2.7
11n		5.46	2.70	6.9
11o		4.28	4.64	1.2
11p		5.12	3.67	1.6
11q		5.00	3.33	4.6
11r		5.49	3.81	0.5
11s		4.43	4.49	1.2
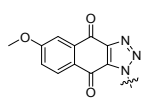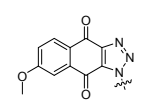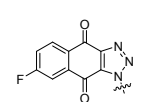
Data for cLogP values were calculated using ChemBioDraw 14 trial. LipE was calculated using LipE = -pIC$_{50}$ (M) - cLogP[43].

To further explore the structure-activity relationship, we further synthesized a series of derivatives by introduction of different substituents to the naphthyl ring of compound **11l**, or replacement of its benzoquinone scaffold with other groups. As
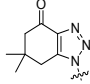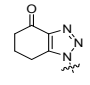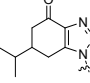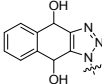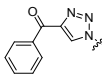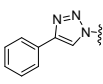
shown in Table 3, most of these final molecules showed reduced activities compared with **11l**. However, compound **14j** (with benzoquinone reduced to tetrahydroxyquinone) maintained comparable potency against *h*DHODH. Nine compounds (**14a–d**, **14g–i** and **14k–l**) displayed a dramatic decrease of over 500 nM in their IC$_{50}$ values. Compounds **14e–f** (IC$_{50}$ = 98 or 152 nM) showed stronger activity than **14a–d**. We deduced that the fluorine atom fit well in the small pocket for compounds **14e–f**. Conversely, compounds **14a–d** (with the larger methoxyl or hydroxyl substituent) clashed with the protein. Replacement of the benzoquinone scaffold of compound **11l** with a cyclohexyl ketone (**14g–i**) or removal of its quinone structural fragment (**14k–l**) diminished *h*DHODH inhibition.

Table 3. Physicochemical Properties and Biological Activity of Compounds 14a–i

Compd	R	clogP	LipE	IC$_{50}$ (nM)
BRQ		6.38	1.9	5.2
11l		5.46	2.88	4.5
14a		5.40	<0.60	>1000
14b		5.40	<0.60	>1000
14c		5.24	<0.76	>1000
14d		5.24	<0.76	>1000
14e		5.61	<0.39	98
14f		5.61	<0.39	152

14g		5.28	<0.72	>1000
14h		4.24	<1.76	>1000
14i		5.69	<0.31	520
14j		3.20	2.10	5.1
14k		5.52	<0.48	>1000
14l		6.33	<-0.33	>1000

Data for cLogP values were calculated using ChemBioDraw 14 trial. LipE was calculated using LipE = -pIC$_{50}$ (M) - cLogP[43].

2.3 Binding mode analysis through the crystal structure of *h*DHODH in complex with compounds 11k, 11l, 11r and 11s

*h*DHODH is composed of a large C-terminal domain and a small N-terminal domain, linked by an extended loop. The large C-terminal domain conceals the redox site in which FMN and the dihydroorotate substrate bind[44]. The N-terminal extension consists of two helices, α1 and α2, harboring the binding site for the cofactor ubiquinone. The helices α1 and α2 form a slot in the so-called hydrophobic patch with the short α1 and α2 loop at the narrow end of the slot. This promotes the formation of a tunnel that ends at the FMN cavity near the α1 and α2 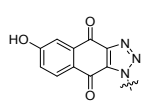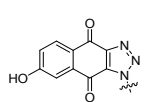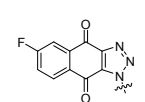loop. This tunnel narrows toward the proximal redox site. A previous study suggested that ubiquinone (cosubstrate) was probably inserted into the tunnel and thus easily approached FMN for the redox reaction[3]. The crystal structures of *h*DHODH in complex with a brequinar analog were recently published[45]. To investigate the binding mode of naphtho[2,3-*d*][1,2,3]triazole-4,9-dione-based inhibitors, the most potent compounds **11k**, **11l**, **11r** **and 11s** were selected for respective cocrystallization with *h*DHODH. The crystal

structures were refined to 1.8 Å resolution, and the coordinates were deposited in the Protein Data Bank as entries 6LP7, 6JME, 6LP8 and 6LP6, respectively. Details of the data collection and refinement statistics are summarized in Table S1. The high resolution and clear density map enabled us to unambiguously determine the position and orientation of these inhibitors (Figure S1), thus revealing the detailed interactions between them and *h*DHODH (Figures 3A, B, E, F). The binding sites of these compounds were clearly in the same pocket, along with the reported inhibitors[24,25,46,47], again supporting the pocket as a rational target for the development of novel inhibitors.

All four inhibitors occupied the proposed putative ubiquinone tunnel, stabilized by a substantial number of hydrophobic interactions with the side chains of *h*DHODH residues lining the pocket (M43, L46, A55, L58, A59, F62, F98, M111, V143, L359, Y356, T360 and P364) (Figures 3A–D). The biphenyl ring system occupied most of the hydrophobic pocket. The naphtho[2,3-*d*][1,2,3]triazole-4,9-dione moiety occupied the innermost part of the pocket near the redox site, including V143, L146, Y356, L359, T360 and P364 (Figures 3A–D). The carbonyl and triazole rings of these compounds formed hydrogen bonds with R136 (Figures 3E–H). Inhibitor **11l** featured a fluorobenzene ring that adopted two different orientations, which accounted for the high potency of compound **11l**. On the basis of the ligand omit map density (Figure S1), the fluorine substituent was directed toward the α1 and α2 helices, and these two conformations had the same occupancy. The methoxy oxygen of **11k** pointed toward the hydroxyl group of Y38 and the carbonyl group of L67 at distances of 3.7 Å and 4.6 Å, respectively, too far to form a direct H-bond. In contrast to compound **11k**, the hydroxyl group of compound **11s** formed hydrogen bonds with the side chain of Y38 and the main chain of L67 (Figure 3G). Compound **11r** formed hydrophobic interactions with Y38 and M111 via the dimethylamino group (Figure 3D). Moreover, we carried out the binding mode assay of A771726, BRQ, Bay-2402234 and compound **11l** with *h*DHODH, and compared their complex structures (Figure S2). The results showed that A771726, BRQ, Bay-2402234 and **11l** all occupied the ubiquinone tunnel, though the amino acid residues that interact with them were not consistent. Hydrophobic interactions were also observed. These results supported the

intrinsic plasticity of binding site with *h*DHODH[48]. Thus, *h*DHODH may accommodate a diverse range of inhibitors, rationalizing the strategy of designing inhibitors with diverse scaffolds.
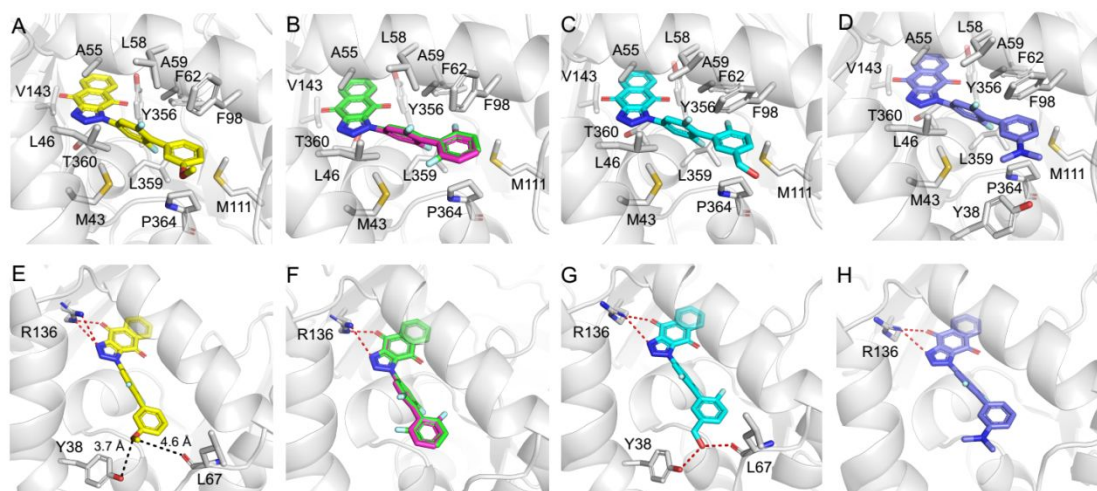
Figure 3. Interaction between *h*DHODH and compounds 11k (yellow PDB 6LP7), 11l (green PDB 6JME), 11s (cyan PDB 6LP6) and 11r (blue PDB 6LP8). Residues that interacted with the inhibitors are labeled and shown as stick representation. (A)–(D) showed the hydrophobic interactions, and (E)–(H) showed the hydrogen bonds (red dashed lines).

2.4 *In vitro* antiproliferative activity of compounds against human cancer cell lines

The proliferation inhibitory effect of the compounds against human cancer cell lines was measured using an MTT assay. BRQ was used as a positive control. The results showed that the cell proliferation inhibitory effects of the compounds were largely related to their solubility and effect on the enzyme inhibitory activity (Table 4). For instance, compounds without any substituent at the diphenyl skeleton (**3s**), or with hydroxyl at meta (**7d**), amino at para (**7e**) or ortho (**7g**) of biphenyl terminal ring which showed moderate inhibition activity against *h*DHODH (IC$_{50}$ = 19-25 nM) only exhibited weaker anti-proliferative effects with IC$_{50}$ values of 0.2-9.04 μM in several cancer cells and > 10 μM in most of cancer cells. Introduction the amino at meta (**7f**), fluorine at ortho (**11a**), methoxyl at meta (**11e**) of biphenyl intermediate ring significantly increased inhibitory potency against *h*DHODH, whereas only slightly

improved the antiproliferative efficacy compared with compounds **7e** and **7g**. The poor membrane permeability or the solubility values might be responsible for the moderate cell proliferation inhibition of compounds **7f**, **11a** and **11e**.

Notably, compounds **11k** and **11l** showed superior antiproliferative activities to BRQ. Compound **11k** exhibited potent anti-proliferative effects against human melanoma A375 cells and human colorectal cancer HCT116 cells with IC_{50} values of 0.04 and 0.60 μM, respectively, and considerable potency against human B-cell lymphoma Raji cells (IC_{50} = 0.48 μM), human chronic myelogenous leukemia K562 cells (IC_{50} = 0.34 μM) and human B-cell lymphoma Nalmawa cells (IC_{50} = 1.04 μM). Compound **11l** displayed more potent activity against A375 and HCT-116, with IC_{50} values of 0.02 and 0.29 μM, respectively, and considerable potency against Raji (IC_{50} = 0.16 μM), K562 (IC_{50} = 0.11 μM) and Nalmawa (IC_{50} = 0.99 μM). These data were consistent with the potent inhibition activity against hDHODH (IC_{50} = 4.5-9 nM) and better solubility (21.4-33.8 μg/ml in PBS) of compounds **11k** and **11l**. On the other hand, compounds with fluorine at para (**11n**), 3'-F (**11m**), 3'-F (**11o**), 3'-CH$_2$OCH$_3$ (**11p**), 3'-CH$_2$COOCH$_3$ (**11q**), 3'-N(CH$_3$)$_2$ (**11r**), 2'-F, 3'-CH$_2$OH (**11s**) of biphenyl terminal ring showed more potent hDHODH activity, but lower cellular bioactivities compared with compounds **11k** and **11l.** Their relatively low inhibitory activity against cancer cells could be attributed to its poor membrane permeability, as observed in the predicted QPPCaco-2 values by Schrodinger_Suites or the poor solubility. Overall, compounds **11k** and **11l** predominantly exhibited proliferation inhibition against cancer cells, which deserves further investigation.

Table 4. Antiproliferation Activity of Compounds against Human Ccancer Cell Lines

Compd	QPPCaco-2[b]	solubility (μg/mL)	MTT Assay (IC$_{50}$[a])							
			A375	HCT116	Hela	A549	MCF-7	Raji	K562	Nalmawa
BRQ	328.45	75.17	0.59	4.12	>10	4.10	>10	2.29	0.54	>10
3s	464.29	nd	5.83	4.23	>10	>10	>10	4.61	>10	1.87

7d	104.75	nd	>10	>10	>10	>10	>10	9.04	7.09	>10
7e	121.01	nd	1.90	>10	>10	>10	>10	>10	0.24	>10
7f	120.92	<10.0	0.25	0.88	>10	>10	>10	1.36	>10	>10
7g	166.98	nd	1.93	2.30	>10	>10	>10	3.84	2.16	5.05
11a	464.23	<10.0	2.98	3.33	>10	>10	>10	2.23	1.87	2.79
11e	561.15	15.4	0.01	0.18	>10	>10	>10	0.79	0.21	>10
11k	465.41	21.4	0.04	0.60	>10	2.25	>10	0.48	0.34	1.04
11l	465.18	33.8	0.02	0.29	>10	1.65	9.61	0.16	0.11	0.99
11m	465.26	<10.0	0.19	0.55	>10	>10	>10	1.51	>10	>10
11n	465.24	nd	1.58	2.25	>10	>10	>10	>10	>10	>10
11o	142.23	14.6	0.03	2.21	>10	>10	>10	3.31	>10	>10
11p	465.19	<10.0	0.18	1.13	>10	>10	>10	1.23	>10	>10
11q	141.42	<10.0	0.42	1.61	>10	>10	>10	3.76	2.41	>10
11r	432.69	<10.0	0.02	0.41	2.02	>10	>10	2.15	>10	>10
11s	142.50	17.6	0.03	0.15	>10	>10	>10	>10	>10	>10
14j	765.20	<10.0	0.16	0.58	>10	>10	>10	>10	>10	>10

[a]IC_{50}, the mean value of triplicate measurements. [b]Data for QPPCaco-2 values were calculated by Schrodinger_Suites.

2.5. Uridine supplementation rescues cell proliferation inhibition induced by compounds 11k and 11l

As the inhibition of hDHODH activity reduces the *de novo* pyrimidine nucleotide synthesis that is vital for cancer cell proliferation, supplementation of exogenous uridine in cancer cells could rescue the proliferation inhibitory effects of hDHODH inhibitors. To evaluate whether the hDHODH inhibition by compounds **11k** and **11l** is mainly responsible for their antiproliferative effect, we carried out uridine supplementation rescue experiments in Raji cells. The results showed that uridine supplementation significantly rescued the cell proliferation inhibition induced by compounds **11k** and **11l** (Figure 4). Interestingly, the rescue effect was more obvious

after compound **11l** treatment than **11k** treatment, which is consistent with the stronger antiproliferation and *h*DHODH inhibitory activity of compound **11l**. Besides *h*DHODH, other enzymes such as carbamoyl phosphate synthetase Ⅱ, aspartate transcarbamoylase and orotate phosphoribosyl transferase (OPRT) are involved in *de novo* pyrimidine biosynthesis. The inhibition of above enzymes may also result in cell proliferation rescue by uridine supplementation. We performed glide-docking experiments and found that both compound **11l** and BRQ can't bind to OPRT (PDB ID :4HKP) which is the only enzymes with crystal structure, suggesting the compound **11l** might not bind to OPRT.

In conclusion, these data demonstrated that compound **11k** and **11l** inhibited cancer cells proliferation by inhibiting *h*DHODH activity.
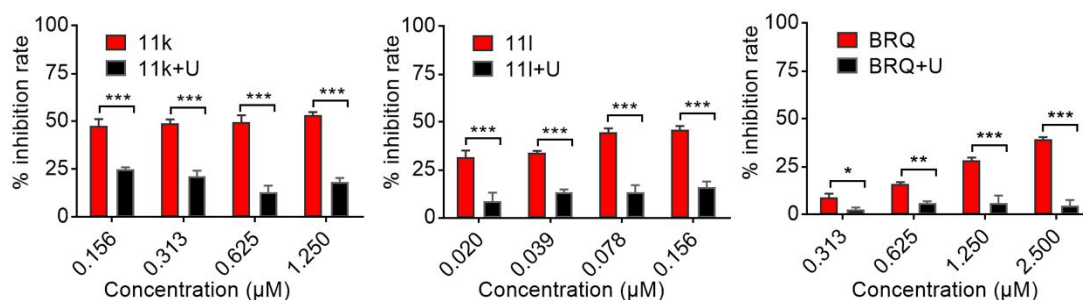
Figure 4. Uridine supplementation rescues Raji cell proliferation inhibition induced by compounds 11k and 11l. Raji cells were treated with **11k**, **11l** or BRQ with or without uridine (U, 500 μM). Data are shown as the mean ± SD. *$p < 0.05$; **$p < 0.01$; ***$p < 0.001$.

2.6. Compounds 11k and 11l induce ROS production and decrease mitochondrial membrane potential

As we aimed to develop an *h*DHODH inhibitor with ROS inducing efficiency, we examined whether compounds **11k** and **11l** could induce the elevation of ROS levels in the Raji cells. The results showed that compounds **11k** or **11l** treatment upregulated the ROS levels in Raji cells in a concentration-dependent manner (Figure 5A). Compared with compounds **11k** or **11l**, the classic *h*DHODH inhibitor BRQ did not increase the ROS level at a concentration of 0.008 μM, and showed less increase at a concentration

of 0.04 μM. These findings suggested that compounds **11k** and **11l** induced more obvious ROS production than the classic *h*DHODH inhibitors. Moreover, we found that compounds **11k** or **11l** induced ROS production at a very low concentration (8 nM), which was similar to that of *h*DHODH inhibition (IC$_{50}$ = 4.5-9 nM). This suggested that compounds **11k** or **11l** directly induced ROS production, but was not dependent on *h*DHODH inhibition. We found that compounds **11k** and **11l** exhibited stronger proliferation inhibitory effect than BRQ, and potent ROS induction effect of compounds **11k** and **11l** might be responsible for this observation. Moreover, we found that BAY-2402234 which has predominant anti-myeloid malignancies potency and high oral bioavailability didn't show inhibitory ability against solid tumor cells. BAY-2402234 is a high specific *h*DHODH inhibitor, whereas compound **11l** could inhibit *h*DHODH activity and induce ROS production as same time, which make it different from BAY-2402234.

As mentioned, both *h*DHODH inhibition and ROS induction can cause mitochondrial dysfunction and exhibit anti-proliferative effects in tumor cells. Loss of mitochondrial membrane potential (ΔΨm) is a character of mitochondrial dysfunction. Thus, the ΔΨm alteration was detected using the mitochondria-specific and voltage-dependent dye tetramethyl rhodamine methyl ester (TMRM). The results show that ΔΨm significantly decreased in a concentration-dependent manner when Raji cells were treated with compound **11k** or **11l** (Figure 5B). Compared with compound **11k** or **11l**, BRQ exhibited less influence on the mitochondrial membrane potential of Raji cells.
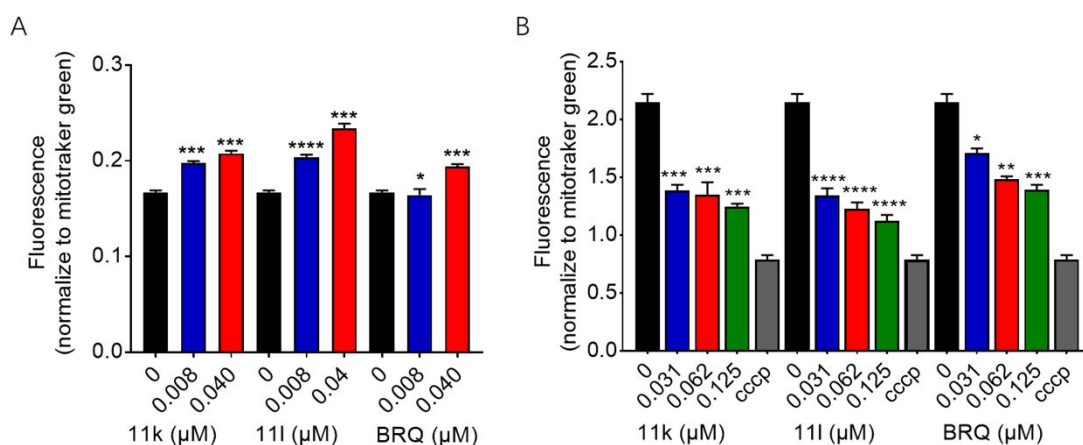
Figure 5. Compounds 11k and 11l induce ROS production and decrease the mitochondrial membrane potential. (A) Raji cells were treated with compounds **11k**, **11l** and BRQ. The ROS level was detected using dihydroethidium. (B) The Raji cells were treated with compounds **11l**, **11k**, BRQ, CCCP (positive control). Mitochondrial dysfunction was detected using TMRM. Data are shown as the mean ± SD. *$p < 0.05$; **$p < 0.01$; ***$p < 0.001$.

2.7. Compounds 11k and 11l induce cell cycle S-phase arrest and apoptosis

As the inhibition of *h*DHODH activity could suppress the formation of pyrimidine nucleotides needed for DNA synthesis, we investigated the influence of compounds **11k** and **11l** on the Raji cell cycle by flow cytometry. The results indicated that compounds **11k** and **11l** significantly induced cell cycle arrest in the S-phase (Figure 6). Compared with 52% of S-phase cells in the control group, compound **11k** at a concentration of 0.5 μM increased the amount of S-phase cells to 77.98%. Compound **11l** at concentrations of 0.031 μM and 0.125 μM increased the amount of S-phase cells to 76.62% and 86.31%, respectively, suggesting that compound **11l** profoundly induced S-phase cell arrest. As a positive control, BRQ showed a weaker effect than **11k** or **11l**.

Then, we further examined the effect of treatment with compounds **11k** and **11l** on apoptosis induction using Annexin V/PI staining assays. We found that compounds **11k** and **11l** induced apoptosis of Raji cells (Figure 7). Compound **11k** treatment exhibited an apoptosis rate of 8.51% at a concentration of 1 μM, and compound **11l** induced an apoptosis rate of 10.14% at concentrations of 0.125 μM. BRQ (1 μM) induced 7.53% apoptosis of Raji cells. These data demonstrated that compounds **11k** and **11l** could induce Raji cell apoptosis, which is consistent with the loss of ΔΨm induced by these two compounds. Taken together, our data demonstrated that compounds **11k** and **11l** effectively induced S-phase arrest and apoptosis in Raji cells.

The studies above showed that compound **11l** exhibited profound efficacy against *h*DHODH activity and cancer cell proliferation *in vitro*. Therefore, we selected compound **11l** for further biological function studies, including pharmacokinetic character, antitumor effect and safety profile *in vivo*.
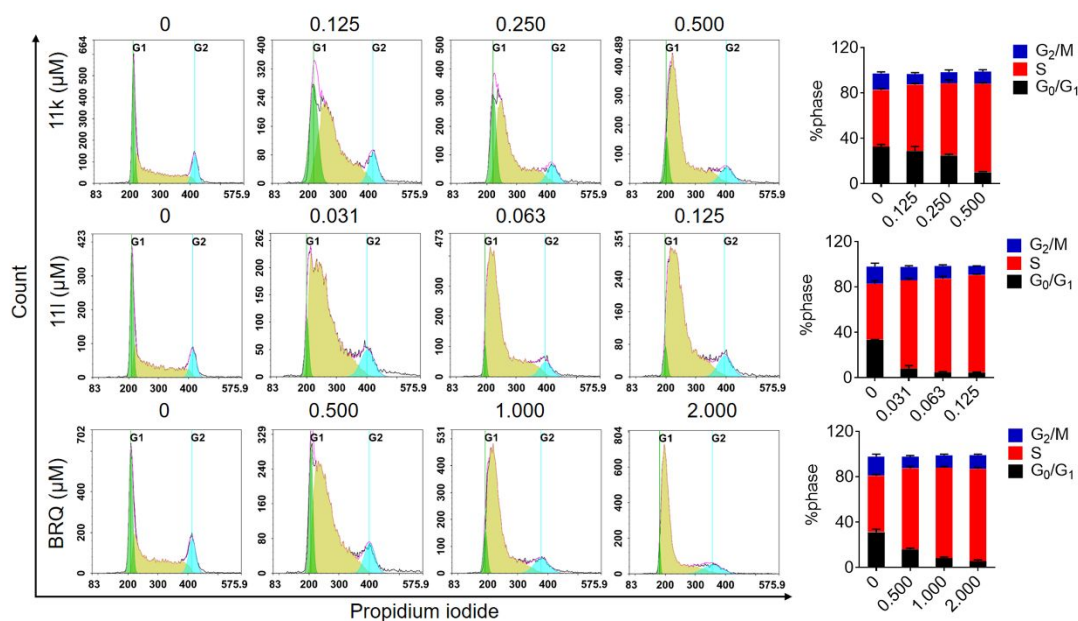
Figure 6. Compounds 11k and 11l induce S-phase cell cycle arrest in Raji cells. Raji cells were treated with various concentrations of compounds **11k**, **11l** or BRQ for 24 h. Cells were stained using PI. Data are shown as the mean ± SD.
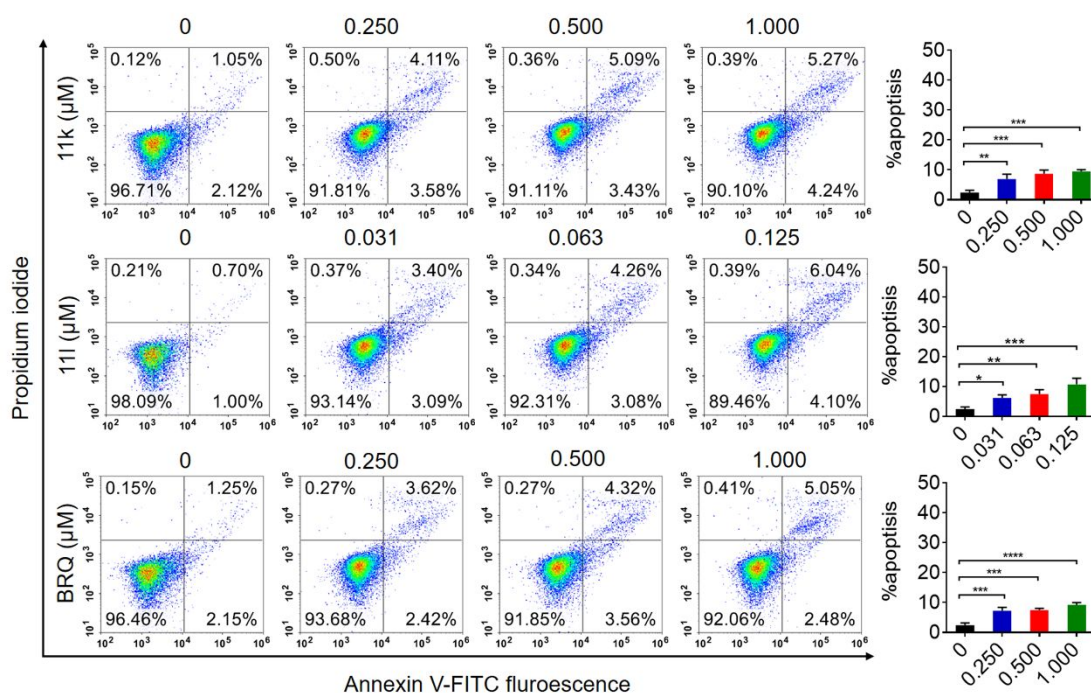
Figure 7. Compounds 11k and 11l induce apoptosis of Raji cells. Raji cells were treated with various concentrations of **11k**, **11l** or BRQ for 48 h. Cells were stained using an Annexin V/FITC Apoptosis Detection Kit. Data are shown as the mean ± SD. $*P < 0.05$; $***P < 0.001$; $****P < 0.0001$.

2.8. Pharmacokinetic character of compound 11l

2.8.1 Nanocrystalline preparation of compound 11l

Our study showed that the lipE and clogP of compound **11l** are 2.88 and 5.46, respectively, which suggested that the solubility of compound **11l** might not be adequate. To better understand the physical property of compound **11l**, we detected its solubility, and the result showed that its solubility in PBS is 33.8 μg/mL (Table S5).

As oral administration is the main administration route for small-molecule anticancer drugs, the solubility of compound **11l** might affect its *in vivo* pharmacokinetic character which is an important part of druggability. Nanotechnology has played a key role in drug delivery and disease treatment owing to its targeted-delivery effect to deal with the problems of low solubility and poor bioavailability of poorly soluble drugs. Therefore, we focused on screening nanocrystalline materials to improve the solubility of compound **11l** and obtain better *in vivo* pharmacokinetic character. Nanocrystalline samples of compound **11l (11l-NC)** were prepared using a microfluidizer (AH100D) as the homogenization device. Compound **11l** (100 mg) was dispersed in a 20 ml aqueous solution of various stabilizers separately (CMC-Na (200 mg), F68 (20 mg) and CA (200 mg) or Tween 20 (240 mg), PEG-4000 (600 mg), CA (100 mg), SDP (50 mg), DSP (100 mg) and NaOH (56.8 mg)) in different concentrations. Samples for characterization were collected after pre-dissolving, as well as after 2, 6, 10, 13, 16 and 20 min of homogenization. The mean particle size (z-average) and polydispersity index (PDI) are summarized in (Table S2). The size and PDI of formulations 1 and 2 were 532.4 or 494.3 nm and 0.142 or 0.256 mV after 20 min, respectively. The results were in line with the requirements of nanocrystalline preparation. Storage stability tests were then performed to assess the effect of temperature or time on the stability of formulations 1 and 2. The results show that the PDI and size variation of formulation 1 were less than those of formulation 2, suggesting that formulation 1 is more stable (Table S3 and S4). Moreover, the formulation 1 resulted in a significant solubility improvement in aqueous buffer form 33.8 to 91.8 μg/ml (Table S5).

2.8.2. Compounds 11l and 11l-NC exhibit good physiological stability

The physiological stability of compounds **11l** and **11l-NC** were evaluated in buffers with pH ranging from 1.0 to 9.0. The results show that the concentration decrease of compounds **11l** and **11l-NC** was between 1.6% and 9% in buffer with pH 1–7.4, and approximately 15% in buffer with pH 9, which suggested that both compounds exhibited good stability in buffers with pH values ranging from 1 to 7.4 (Table S6). However, the concentration decrease of BRQ was between 6.3% and 12.1% in buffer with pH 1–7.4, and 75.4% in buffer with pH 9. This result suggests that compounds **11l** and **11l-NC** were more stable than BRQ (Table S6).

2.8.3 *In Vivo* evaluation of oral bioavailability

The oral bioavailability of compound **11l** and its nanocrystalline preparation (**11l-NC**) were assessed on Sprague-Dawley (SD) rats after their oral (po) or intravenous (iv) administration. Pharmacokinetic (PK) parameters are summarized in Table 5. Compared with compound **11l**, oral administration of **11l-NC** obtained a longer half-life ($T_{1/2}$, h) (8.83 vs 12.47) and a larger area under the concentration-time curve ($AUC_{0-\infty}$, µg/L·h) (4879 vs 141075). The oral maximum plasma concentration (C_{max}) of **11l-NC** was 6369 µg/L, which was larger than compound **11l**. Importantly, **11l-NC** exhibited an improved oral bioavailability of 25.16%, which is 2.6-fold larger than that of compound **11l**.

Table 5. Pharmacokinetic Parameters of Compounds 11l and 11l-NC after Oral or Intravenous Administration

|	Route	$AUC_{(0-t)}$ (µg/L·h)	$AUC_{(0-\infty)}$ (µg/L·h)	CLz/F (L/h/kg)	$T_{1/2}$ (h)	T_{max} (h)	C_{max} (µg/L)	oral F (%)
11l	iv	8414	8417	0.62	3.89	0.08	9450	
	po	4879	6825	5.47	8.83	10	279	9.66
11l-NC	iv	95721	142632	0.08	12.01	0.08	76941	
	po	141075	215279	0.18	12.47	27	6369	25.16

Expressed as mean, n = 6.

2.8.4. Microsome stability of compounds 11l and 11l-NC

The microsome stabilities of **11l** and **11l-NC** were evaluated using *in vitro* liver microsome preparations from human, rat and mouse. The results show the clearances of **11l-NC** and **11l** were 1.03 vs 2.63, 1.53 vs 4.21 and 1.52 vs 2.28 mL/min/kg in human, rat and mouse liver microsomes, respectively (Table S7). The parameter analysis showed that the $T_{1/2}$ of **11l-NC** and **11l** was 63 vs 32, 54 vs 19.8 and 50 vs 37 min in human, rat and mouse liver microsomes, respectively (Table S7). These data indicated that **11l-NC** exhibited an encouraging level of microsomal stability compared with compound **11l**.

2.9. Compounds 11l and 11l-NC inhibit Raji tumor growth *in vivo*

The *in vivo* antitumor efficacy of compounds **11l** and **11l-NC** was evaluated with mouse subcutaneous xenograft models. Nude mice carrying Raji xenograft tumors were orally administered compound **11l** (30 mg/kg), **11l-NC** (40, 80 mg/kg) and BRQ (10 mg/kg). Tumor volumes and body weights were measured every 3 days. The results show that compound **11l** inhibited tumor growth with a growth inhibition rate of 42% (Figure S3). Compared with compound **11l**, **11l-NC** exhibited a more obvious inhibition of tumor growth without decrease of body weight. The inhibition rate for 40 and 80 mg/kg **11l-NC** were 52% and 68%, respectively (Figure 8). In contrast, although BRQ treatment significantly reduced tumor growth with an inhibition rate of 74%, BRQ treatment induced obvious body weight loss and liver damage (Figure 8, S4). Moreover, no obviously adverse effects were observed during treatment with compounds **11l** and **11l-NC**, such as toxic death, dermatitis, or body weight loss. Raji cell lines are human Burkitt's lymphoma (BL) cell lines which are intensively used in BL research. BL is a rare, highly aggressive subtype of non-Hodgkin lymphoma.   Treatment options for relapsed and refractory BL remain limited. Thus, novel therapy strategy for BL treatment will be helpful for BL patients[49]. Collectively, **11l-NC** significantly inhibited tumor growth *in vivo* and exhibited greater safety than BRQ.
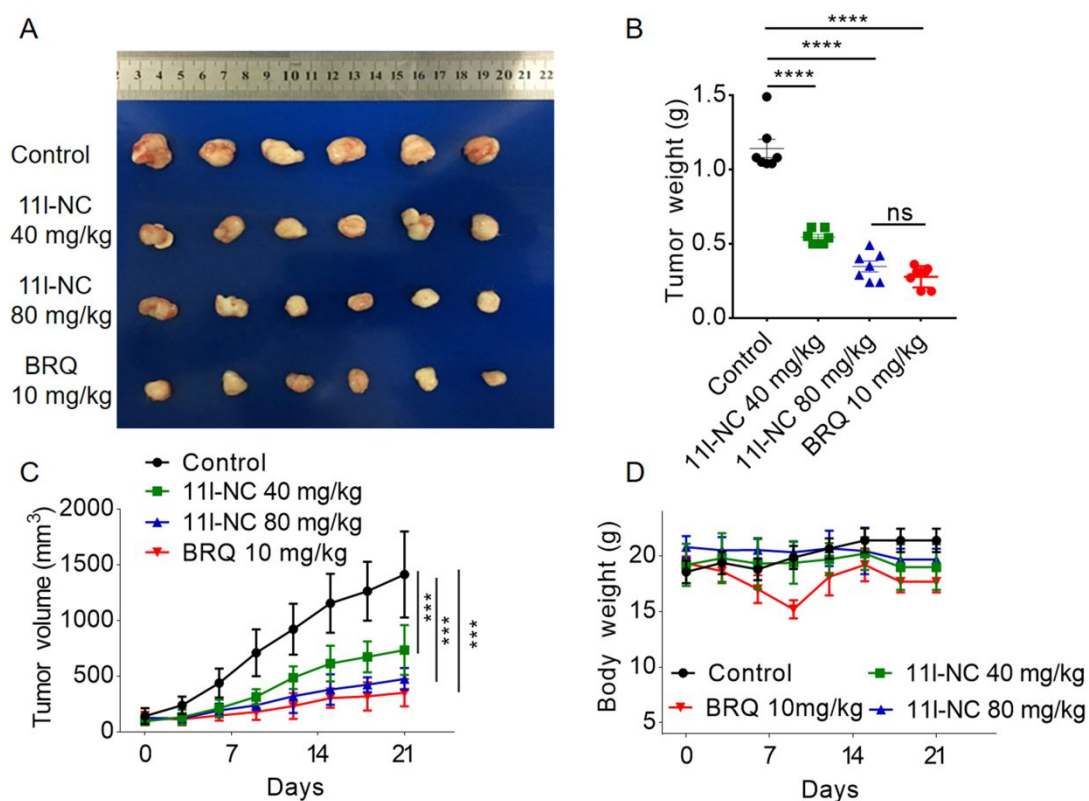
Figure 8. **11l-NC inhibits Raji tumor growth** *in vivo*. Oral administration of **11l-NC** (40 or 80 mg kg^{-1} d^{-1}) and BRQ (10 mg kg^{-1}) were initiated when the Raji tumor volume reached 100–200 mm^3 (six mice per group), 6 days per week for 3 weeks. (A) Representative images of tumor. (B) Tumor weight. (C) Tumor volume. (D) Mice body weight. The data are shown as the mean ± SD. *$P < 0.05$; **$P < 0.01$; ***$P < 0.001$; ****$P < 0.0001$.

2.10. Safety profile of compounds 11l and 11l-NC *in vivo*

An acute toxicity assay was performed to detect the maximum tolerated dose (MTD), which was used to determine the highest dosage of compounds **11l** and **11l-NC** that does not cause obvious side effects. **11l-NC** had a higher MTD value (800 mg/kg) compared with **11l** (400 mg/kg). No significant differences of blood biochemical parameters (including ALT, AST, TP, ALB, BILT, ALP, GLU, BUN, CREA, UA, CHO1, TG, CK, LDH, HDL and LDLC) were observed after compounds **11l** and **11l-NC** treatment (Figure 9). Consistent with previous reports, BRQ exhibited dose-dependent toxicity as measured by body weight loss in the treated mice. At the 30

mg/kg dose, this body weight loss was large enough to require termination of that arm of the study[50-52].

The high safety property and inhibitory against hDHODH of compound **11l** are quite encouraging. The hDHODH inhibitors could be used for treatment of rheumatoid arthritis and psoriatic arthritis besides malignant tumor[53]. Moreover, hDHODH inhibitor exhibited inhibitory activity against PfDHODH. For example, A771726, a hDHODH inhibitor ($IC_{50} = 261$ nM) could inhibit PfDHODH activity with an IC_{50} value of 191 μM[54]. These studiessuggested that compounds with hDHODH inhibitory activity may inhibit the activity PfDHODH though the efficacy is weak[54-56]. Thus, the series described in our work may be used for treatment of rheumatoid arthritis, psoriatic arthritis and growth of *P. falciparum* and further studies are needed.
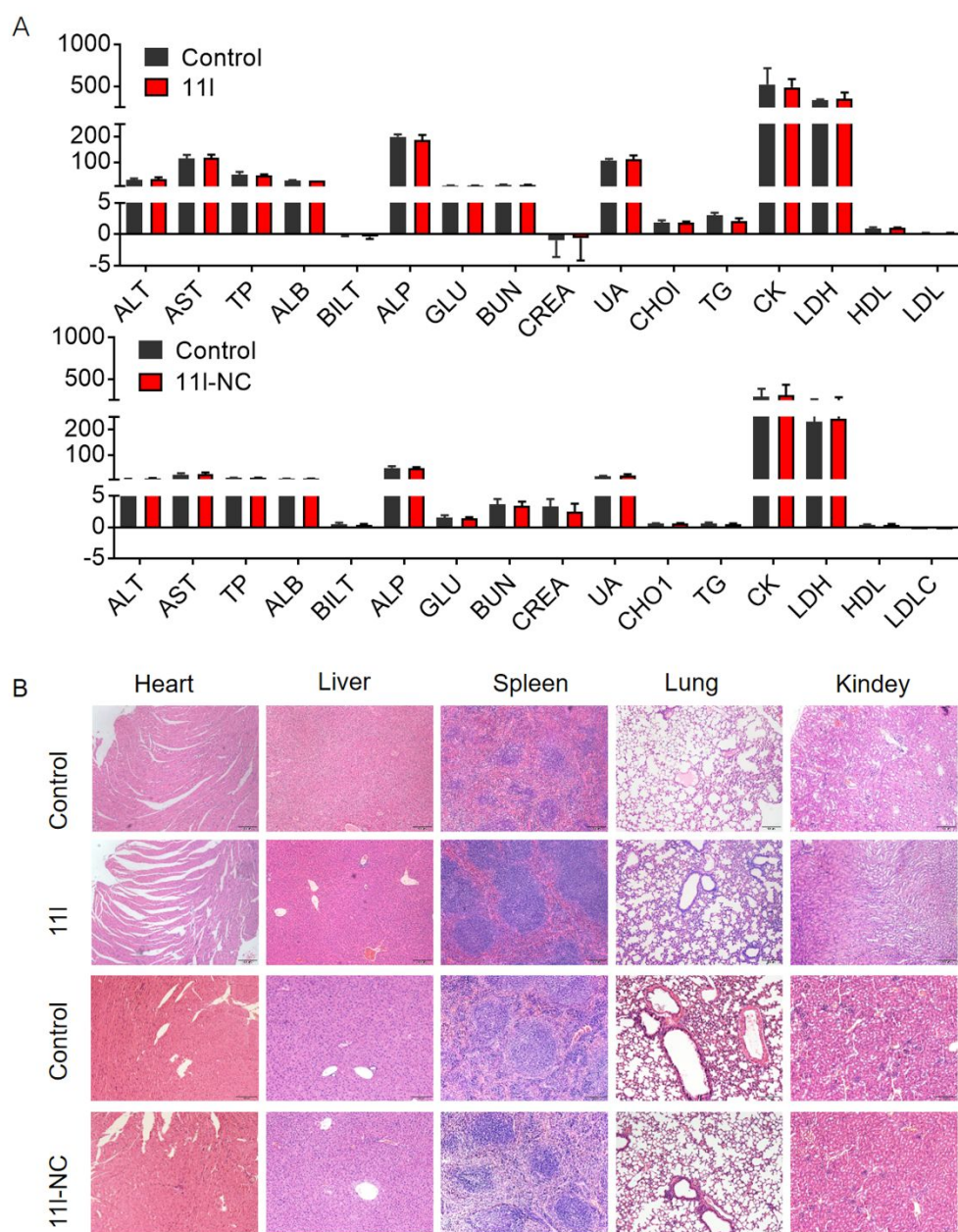
Figure 9. No significant change of blood biochemical assay and H&E staining of main organs after compounds 11l and 11l-NC treatment in acute toxic assay. BALB/c mice were orally administrated with **11l** (400 mg/kg) and **11l-NC** (800 mg/kg) within 24 hours. (A) Blood biochemical assay at the end of treatment. (B) Representative H&E staining images of main organs. The data are shown as the mean ± SD.

CONCLUSION

In this study, a series of novel hDHODH inhibitors with ROS-inducing capacity

with a naphtho[2,3-*d*][1,2,3]triazole-4,9-dione scaffold was designed and synthesized. An initial medicinal chemistry campaign led to the identification of a potent compound **3s** (*h*DHODH IC$_{50}$ = 19 nM). Further optimization obtained compounds including compounds **11k** and **11l,** which had favorable enzymatic activity (*h*DHODH IC$_{50 =}$ 9.0 and 4.5 nM, respectively) and cellular activities (Raji: IC$_{50}$ = 0.48 and 0.16 μM, respectively). Ligand-protein cocrystal structures depict an exclusive H-bonding interaction with the R136 residue. Mechanism study showed that compounds **11k** and **11l** induced ROS production, mitochondrial dysfunction, apoptosis and cell cycle S-phase arrest. Remarkably, compound **11l-NC** exhibited significant growth inhibition and favorable safety profile *in vivo*. Taken together, we developed naphtho[2,3-*d*][1,2,3]triazole-4,9-dione compounds as a new class of *h*DHODH inhibitors with ROS production activity. Future studies will evaluate the capability of the inhibitors to inhibit various tumor growths *in vivo*, and seek to improve oral bioavailability through prodrug design strategies.

EXPERIMENTAL SECTION

Chemistry Methods. All reagents and solvents were obtained from commercial suppliers and used without further purification. Anhydrous solvents were dried and purified by conventional methods prior to use. Brequinar (BRQ) was purchased from the commercial source MedChemExpress. Column chromatography was carried out on silica gel (200-300 mesh). Thin-layer chromatography (TLC) was carried out to monitor reaction progress, and silica gel plates with F-254 fluorescence were used and visualized with UV light. ^{1}H NMR and ^{13}C NMR spectra were obtained using a Bruker AV-400 spectrometer at 400 and 101 MHz, respectively. Spectral data are reported using the following abbreviations: Coupling constants (J) are expressed in hertz (Hz). s = singlet, d = doublet, t = triplet, q = quartet, m = multiplet, dd = doublet of doublets. Chemical shifts (δ) are listed in parts per million (ppm) relative to tetramethylsilane (TMS) as an internal standard. Biological experiments were performed on final compounds with a purity of at least 95%. Purity was checked using a highperformance on Waters 2695 series chromatograph. Mass spectrometry (MS) data were acquired on

a Waters Q-TOF Premier mass spectrometer (Micromass, Manchester, U.K.).

2-{4,9-Dioxo-1*H*,4*H*,9*H*-naphtho[2,3-*d*][1,2,3]triazol-1-yl}benzonitrile (3a). A mixture of 2-Hydroxy-1,4-naphoquinone (120 mg, 0.69 mmol), 2-azidobenzonitrile (99 mg, 0.69 mmol) DBU (10 mol %), in CH_3CN (3 mL) were stirred at 80 ℃ for 3-4 h. the reaction was quenched with water and extracted with dichloromethane (3 × 100 mL) . The combined organic layer was washed with brine, and then evaporated in vacuo. The crude product was purified using silica gel chromatography with a petroleum ether /dichloromethane gradient to afford the desired product as a white solid. (96 mg, 34.5% yield). ^{1}H NMR (400 MHz, DMSO-d_6) δ 8.30–8.24 (m, 2H), 8.12 (dd, J = 7.4, 1.6 Hz, 1H), 8.09–7.92 (m, 5H).^{13}C NMR (101 MHz, DMSO-d_6) δ 176.73, 173.91, 144.72, 136.30, 135.35, 134.80, 134.59, 134.17, 132.91, 132.86, 131.88, 128.32, 127.10, 126.96, 115.07, 109.25. HRMS m/z (ESI) calcd for $C_{17}H_9N_5O_2$ [M + Na]$^+$ 323.0647; found, 323.0547. Compounds **3b-t**,**7a-g**,**11a-s** were synthesized by using a similar procedure.

3-{4,9-Dioxo-1*H*,4*H*,9*H*-naphtho[2,3-*d*][1,2,3]triazol-1-yl}benzonitrile (3b). White solid (36% yield). ^{1}H NMR (400 MHz, DMSO-d_6) δ 8.41 (t, J = 1.6 Hz, 1H), 8.28–8.24 (m, 1H), 8.18 (dddd, J = 5.6,3.2, 2.0,1.2 Hz, 3H), 7.98 (pd, J =9.2, 1.6 Hz, 2H), 7.92 (t, J = 8.4 Hz, 1H).^{13}C NMR (101 MHz, DMSO-d_6) δ 176.92, 173.96, 144.84, 135.72, 135.16, 134.91, 134.82, 134.42, 133.16, 132.66, 130.80, 130.32, 129.11, 127.12, 126.96, 112.16. HRMS m/z (ESI) calcd for $C_{17}H_8N_4O_2$ [M + Na]$^+$ 323.0647; found, 323.00528.

1-(3-Hydroxyphenyl)-1*H*,4*H*,9*H*-naphtho[2,3-*d*][1,2,3]triazole-4,9-dione (3c). White solid (39% yield). ^{1}H NMR (400 MHz, DMSO-d_6) δ 8.29–8.20 (m, 1H), 8.16–8.07 (m, 1H), 7.96 (dd, J =6.4,1.2 Hz, 2H), 7.44 (t, J = 8.0 Hz, 1H), 7.23–7.12 (m, 2H), 7.09–6.97 (m, 1H), 6.17 (d, J = 7.6 Hz, 1H).^{13}C NMR (101 MHz, DMSO-d_6) δ 176.73, 173.91, 144.72, 136.30, 135.35, 134.80, 134.59, 134.17, 132.91, 132.86, 131.88, 128.32, 127.10, 126.96, 115.07, 109.25. HRMS m/z (ESI) calcd for $C_{16}H_9 N_3O_2$ [M + Na]$^+$ 314.0644; found, 314.0537.

1-(2-Methoxyphenyl)-1*H*,4*H*,9*H*-naphtho[2,3-*d*][1,2,3]triazole-4,9-dione (3d). White solid (24% yield). ^{1}H NMR (400 MHz, DMSO-d_6) δ 8.24 (d, J = 7.5 Hz, 1H),

8.08 (d, J = 7.5 Hz, 1H), 7.96 (dd, J = 12.4, 7.4 Hz, 2H), 7.68 (t, J = 7.9 Hz, 1H), 7.60 (d, J = 7.5 Hz, 1H), 7.38 (d, J = 8.3 Hz, 1H), 7.21 (t, J = 7.6 Hz, 1H), 3.76 (s, 3H).^{13}C NMR (101 MHz, DMSO-d_6) δ 177.56, 174.41, 163.12, 160.66, 145.32, 135.48, 135.18, 133.77, 133.24, 131.77, 129.15, 127.51, 127.35 126.04, 116.32, 116.08, 14.62.HRMS m/z (ESI) calcd for $C_{17}H_{11}N_3O_3$ [M + Na]$^+$ 328.0800; found, 328.0709.

1-(3-Iodophenyl)-1H,4H,9H-naphtho[2,3-d][1,2,3]triazole-4,9-dione (3e). White solid (39% yield). ^{1}H NMR (400 MHz, CDCl$_3$) δ 8.39 (d, J = 8.0 Hz, 1H), 8.24 (d, J = 7.2 Hz, 1H), 8.13 (s, 1H), 7.97 (d, J = 8.0 Hz, 1H), 7.87 (dd, J = 7.2 , 4.8 Hz, 2H), 7.75 (d, J = 8.0 Hz, 1H), 7.36 (t, J = 8.0 Hz, 1H). ^{13}C NMR (101 MHz, CDCl$_3$) δ 177.05, 174.16, 147.42, 136.22, 135.07, 134.47, 133.27, 133.04, 132.11, 131.45, 130.01, 127.70, 127.65, 117.11, 114.77, 111.19. HRMS m/z (ESI) calcd for $C_{16}H_8IN_3O_2$ [M + Na]$^+$ 423.9661; found, 423.9558.

1-(3-Aminophenyl)-1H,4H,9H-naphtho[2,3-d][1,2,3]triazole-4,9-dione (3f). White solid (42% yield). ^{1}H NMR (400 MHz, CDCl$_3$) δ 8.38 (dd, J = 7.6, 1.2 Hz, 1H), 8.22 (dd, J = 7.2, 1.4 Hz, 1H), 7.96–7.60 (m, 2H), 7.36 (t, J = 8.0 Hz, 1H), 7.12–7.03 (m, 1H), 7.01 (t, J = 2.2 Hz, 1H), 6.90 (dd, J = 8.14, 2.0 Hz, 1H), 3.97 (s, 2H). ^{13}C NMR (101 MHz, CDCl$_3$) δ 177.05, 174.16, 147.42, 136.22, 135.07, 134.47, 133.27, 133.04, 132.31, 131.25, 130.01, 127.70, 127.65, 117.11, 114.77, 111.19.HRMS m/z (ESI) calcd for $C_{16}H_{10}N_4O_2$ [M + Na]$^+$ 313.0804; found,313.0703.

1-[4-(Propan-2-yl)phenyl]-1H,4H,9H-naphtho[2,3-d][1,2,3]triazole-4,9-dione (3g). White solid (34% yield). ^{1}H NMR (400 MHz, DMSO-d_6) δ 8.25–8.20 (m, 1H), 8.14–8.09 (m, 1H), 8.00–7.91 (m, 2H), 7.72 (d, J = 8.4 Hz, 2H), 7.54 (d, J = 8.4 Hz, 2H), 3.06 (dt, J = 13.8, 6.6 Hz, 1H), 1.30 (d, J = 6.8 Hz, 6H).^{13}C NMR (101 MHz, DMSO) δ 177.11, 173.91, 151.12, 144.96, 134.91, 134.65, 134.43, 133.36, 133.09, 132.75, 127.01, 126.99, 126.81, 125.24, 33.30, 23.69. HRMS m/z (ESI) calcd for $C_{19}H_{15}N_3O_2$ [M + H]$^+$ 317.1164; found, 318.1234.

1-[2-(Trifluoromethyl)phenyl]-1H,4H,9H-naphtho[2,3-d][1,2,3]triazole-4,9-dione (3h). White solid (51% yield). ^{1}H NMR (400 MHz, DMSO-d_6) δ 8.27 (d, J = 7.6 Hz, 1H), 8.14 (d, J = 7.2 Hz, 1H), 8.07 (d, J = 7.6 Hz, 1H), 8.01 (t, J = 7.8 Hz, 3H), 7.98–7.93 (m, 1H), 7.90 (d, J = 7.6 Hz, 1H). ^{13}C NMR (101 MHz, DMSO-d_6) δ 177.22,

174.39, 144.80, 136.55, 135.91, 135.24, 134.60, 133.55, 133.08, 132.84 (d, J = 1.01 Hz), 132.75, 130.36, 128.05(dd, J = 5.05 Hz), 127.64, 127.35, 125.97(d, J = 31.31 Hz), 124.49(d, J = 274.72 Hz).HRMS m/z (ESI) calcd for $C_{17}H_8F_3N_3O_2$ [M +Na]$^+$ 366.0569; found, 366.0460.

1-(4-Fluoro-3-methylphenyl)-1*H*,4*H*,9*H*-naphtho[2,3-*d*][1,2,3]triazole-4,9-dione (3i). White solid (55% yield). ^{1}H NMR (400 MHz, DMSO-d_6) δ 8.27–8.23 (m, 1H), 8.15–8.11 (m, 1H), 7.96 (pd, J = 7.4, 1.6 Hz, 2H), 7.78 (dd, J = 6.6, 2.4 Hz, 1H), 7.72–7.67 (m, 1H), 7.46 (t, J = 9.2 Hz, 1H), 2.36 (d, J = 1.8 Hz, 3H). ^{13}C NMR (101 MHz, DMSO-d_6) δ 177.07, 173.92, 162.63, 160.17, 144.83, 134.69 (d, J = 6.06 Hz), 133.28, 132.75, 131.28 (d, J = 3.03 Hz), 128.66(d, J = 6.06 Hz), 127.02 (d, J = 16.16 Hz), 125.74, 125.55, 125.21 (d, J = 9.09 Hz), 115.83, 115.59, 14.13 (d, J = 3.03 Hz).HRMS m/z (ESI) calcd for $C_{17}H_{10}FN_3O_2$ [M + Na]$^+$ 330.0757; found, 330.0612.

1-[4-Methyl-3-(trifluoromethyl)phenyl]-1*H*,4*H*,9*H*-naphtho[2,3-*d*][1,2,3]triazole-4,9-dione (3j). White solid (51% yield). ^{1}H NMR (400 MHz, DMSO-d_6) δ 8.29–8.26 (m, 1H), 8.14–8.10 (m, 1H), 7.96 (pd, J = 7.4, 1.6 Hz, 2H), 7.78 (dd, J = 6.6, 2.4 Hz, 1H), 7.72–7.67 (m, 1H), 7.46 (t, J = 9.2 Hz, 1H), 2.36 (d, J = 1.8 Hz, 3H) .^{13}C NMR (101 MHz, DMSO) δ 177.56, 174.41, 163.12, 160.66, 145.32, 135.48, 135.18(d, J = 5.05 Hz), 133.77, 133.24, 131.77 (d, J = 3.03 Hz), 129.15 (d, J = 6.06 Hz), 127.51 (d, J = 16.16 Hz), 126.23, 126.04, 125.70, 125.61, 116.32, 14.62. HRMS m/z (ESI) calcd for $C_{18}H_{10}F_3N_3O_2$ F[M + Na]$^+$ 380.0725; found, 380.0614.

1-(6-Chloropyridin-3-yl)-1*H*,4*H*,9*H*-naphtho[2,3-*d*][1,2,3]triazole-4,9-dione (3k). White solid (46% yield). ^{1}H NMR (400 MHz, DMSO-d_6) δ 8.93 (s, 1H), 8.51–8.32 (m, 1H), 8.27 (d, J = 7.2 Hz, 1H), 8.15 (d, J = 6.8 Hz, 1H), 8.04–7.95 (m, 2H), 7.93 (d, J = 8.0 Hz, 1H).^{13}C NMR (101 MHz, DMSO-d_6) δ 176.84, 174.03, 151.74, 146.15, 144.86, 136.71, 135.25, 134.87, 133.07, 132.69, 131.61, 131.16, 127.09, 127.02, 124.91. HRMS m/z (ESI) calcd for $C_{15}H_7ClN_4O_2$ [M + Na]$^+$333.0258; found, 333.0155.

1-(2-Chloropyridin-4-yl)-1*H*,4*H*,9*H*-naphtho[2,3-*d*][1,2,3]triazole-4,9-dione (3l). White solid (61% yield). ^{1}H NMR (400 MHz, CDCl$_3$) δ 8.68 (d, J = 5.2 Hz, 1H), 8.38 (dd, J = 6.4, 1.2 Hz, 1H), 8.26 (dd, J = 7.6, 1.2 Hz, 1H), 7.94–7.83 (m, 3H), 7.80 (dd, J = 5.6, 1.6 Hz, 1H).^{13}C NMR (100 MHz, CDCl$_3$) δ 176.44, 174.13, 152.84, 150.99,

146.43, 143.90, 135.66, 134.86, 133.12, 132.87, 132.70, 128.01, 127.92, 119.32, 117.37.HRMS m/z (ESI) calcd for $C_{17}H_8ClN_4O_2$ [M + Na]$^+$ 333.0258; found, 333.0188.

1-(Pyridin-4-yl)-1H,4H,9H-naphtho[2,3-d][1,2,3]triazole-4,9-dione (3m). White solid (45% yield). ^{1}H NMR (400 MHz, CDCl$_3$) δ 8.98–8.90 (m, 2H), 8.44–8.36 (m, 1H), 8.29–8.24 (m, 1H), 7.95–7.82 (m, 4H). ^{13}C NMR (101 MHz, CDCl$_3$) δ 176.76, 174.33, 151.50, 146.54, 142.32, 135.65, 134.90, 133.63, 133.12, 132.94, 128.03, 128.01, 118.75. HRMS m/z (ESI) calcd for $C_{15}H_8N_4O_2$ [M + Na]$^+$ 299.0647; found, 299.0534.

1-(Naphthalen-2-yl)-1H,4H,9H-naphtho[2,3-d][1,2,3]triazole-4,9-dione (3n). White solid (41% yield). ^{1}H NMR (400 MHz, DMSO-d_6) δ 8.45 (d, J = 1.6 Hz, 1H), 8.29–8.25 (m, 1H), 8.22 (d, J = 8.8 Hz, 1H), 8.13 (dd, J = 5.6, 3.2 Hz, 3H), 7.97 (dq, J = 7.2, 5.6 Hz, 2H), 7.90 (dd, J = 8.8, 2.0 Hz, 1H), 7.76–7.68 (m, 2H). ^{13}C NMR (100 MHz, DMSO-d_6) δ177.64, 174.49, 145.53, 135.48, 135.28, 135.19, 133.86, 133.78, 133.30, 133.23, 132.71, 129.49, 129.07, 128.42, 127.96, 127.54, 127.41, 127.37, 124.89, 123.39. HRMS m/z (ESI) calcd for $C_{20}H_{11}N_3O_2$ [M + Na]$^+$ 348.0851; found, 348.0749.

1-(2H-1,3-Benzodioxol-5-yl)-1H,4H,9H-naphtho[2,3-d][1,2,3]triazole-4,9-dione (3o). White solid (49% yield). ^{1}H NMR (400 MHz, DMSO-d_6) δ 8.27–8.22 (m, 1H), 8.16–8.11 (m, 1H), 8.03–7.92 (m, 2H), 7.41 (d, J = 2.0 Hz, 1H), 7.29 (dd, J = 8.0, 2.0 Hz, 1H), 7.17 (d, J = 8.3 Hz, 1H), 6.23 (s, 2H).^{13}C NMR (101 MHz, DMSO-d_6) δ 163.56, 156.29, 147.20, 141.69, 134.94, 134.68, 133.36, 133.15, 132.78, 130.90, 128.91, 127.13, 126.90, 119.59, 108.04, 106.69, 102.37. HRMS m/z (ESI) calcd for $C_{17}H_9N_3O_4$ [M + Na]$^+$ 342.0593; found, 342.0485.

1-(1H-1,3-Benzodiazol-2-yl)-1H,4H,9H-naphtho[2,3-d][1,2,3]triazole-4,9-dione (3p). White solid (40% yield). ^{1}H NMR (400 MHz, DMSO-d_6) δ 7.90–7.85 (m, 2H), 7.72 (td, J = 7.5, 1.4 Hz, 1H), 7.62 (td, J = 7.5, 1.4 Hz, 1H), 7.32–7.20 (m, 3H), 7.03 (dd, J = 5.8, 3.2 Hz, 2H).^{13}C NMR (101 MHz, DMSO-d_6) δ 185.08, 181.75, 167.87, 152.88, 134.50, 134.15, 133.61, 131.39, 131.11, 125.30, 124.94, 120.97, 111.41, 108.11. HRMS m/z (ESI) calcd for $C_{17}H_9N_5O_2$ [M + Na]$^+$ 338.0756; found, 338.0642.

1-[4-(Pyridin-3-yl)phenyl]-1H,4H,9H-naphtho[2,3-d][1,2,3]triazole-4,9-dione (3q).

White solid (48% yield). ^{1}H NMR (400 MHz, CDCl$_3$) δ 8.95 (d, J = 2.0 Hz, 1H), 8.69 (dd, J = 3.6, 2.4 Hz, 1H), 8.40 (dd, J = 6.8, 1.2 Hz, 1H), 8.25 (dd, J = 6.8, 0.8 Hz, 1H), 8.00–7.96 (m, 1H), 7.92–7.81 (m, 6H), 7.45 (dd, J = 4.8, 3.2 Hz, 1H).^{13}C NMR (101 MHz, CDCl$_3$) δ 176.90, 174.40, 149.46, 148.38, 146.06, 140.51, 135.30, 135.10, 134.59, 134.56, 134.21, 133.37, 133.20, 133.15, 133.07, 128.14, 127.99, 127.83, 127.71, 125.73, 123.78. HRMS m/z (ESI) calcd for C$_{21}$H$_{12}$N$_4$O$_2$ [M + H]$^+$ 353.0960; found, 353.1031; calcd for C$_{21}$H$_{12}$N$_4$O$_2$ [M + Na]$^+$ 375.0854; found, 375.0854.

1-[4-(Pyridin-4-yl)phenyl]-1*H*,4*H*,9*H*-naphtho[2,3-*d*][1,2,3]triazole-4,9-dione (3r).
White solid (42% yield). ^{1}H NMR (400 MHz, CDCl$_3$) δ 8.75 (dd, J = 2.8, 1.6 Hz, 2H), 8.40 (dd, J = 6.4, 1.2 Hz, 1H), 8.25 (dd, J = 6.4, 1.2 Hz, 1H), 7.94–7.82 (m, 7H), 7.60 (dd, J = 3.2, 1.6 Hz, 2H).^{13}C NMR (101 MHz, CDCl$_3$) δ 177.04, 174.54, 149.60, 148.52, 146.20, 140.65, 135.44, 135.24, 134.73, 134.70, 133.51, 133.21, 128.14, 127.97, 126.85, 125.87, 123.92.HRMS m/z (ESI) calcd for C$_{21}$H$_{12}$N$_4$O$_2$ [M + Na]$^+$ 375.0960; found, 375.0858.

1-{[1,1'-Biphenyl]-4-yl}-1*H*,4*H*,9*H*-naphtho[2,3-*d*][1,2,3]triazole-4,9-dione   (3s).
White solid (41% yield). ^{1}H NMR (400 MHz, DMSO-d_6) δ 8.27 (dd, J = 5.6, 1.6 Hz, 1H), 8.16 (dd, J = 6.8, 1.7 Hz, 1H), 8.03–7.94 (m, 4H), 7.92 (d, J = 8.8 Hz, 2H), 7.85–7.80 (m, 2H), 7.56 (t, J = 7.4 Hz, 2H), 7.47 (t, J = 7.2 Hz, 1H). ^{13}C NMR (101 MHz, DMSO-d_6) δ 177.12, 173.98, 142.27, 138.76, 134.70, 134.57, 134.45, 133.39, 133.07, 132.77, 129.13, 128.26, 127.37, 127.18, 127.02, 126.96, 126.86, 125.87. HRMS m/z (ESI) calcd for C$_{22}$H$_{13}$N$_2$O$_3$ [M + Na]$^+$374.1008; found, 374.0864.

1-[6-(Morpholin-4-yl)pyridin-3-yl]-1*H*,4*H*,9*H*-naphtho[2,3-*d*][1,2,3]triazole-4,9-dione (3t). White solid (47% yield). ^{1}H NMR (400 MHz, DMSO-d_6) δ 8.51 (d, J = 2.4 Hz, 1H), 8.24 (d, J = 6.8 Hz, 1H), 8.12 (s, 1H), 7.96 (dd, J = 10.0, 4.4 Hz, 3H), 7.07 (d, J = 9.2 Hz, 1H), 3.75 – 3.63 (m, 4H), 3.64–3.61 (m, 4H). ^{13}C NMR (101 MHz, DMSO-d_6) δ 177.01, 174.08, 159.27, 144.80, 144.01, 134.98, 134.67, 134.55, 134.16, 133.26, 132.81, 131.55, 126.88, 122.56, 106.12, 65.87, 44.84. HRMS m/z (ESI) calcd for C$_{19}$H$_{15}$N$_5$O$_3$ [M + Na]$^+$ 361.1175; found, 384.1070.

1-[4-(Pyrimidin-5-yl)phenyl]-1*H*,4*H*,9*H*-naphtho[2,3-*d*][1,2,3]triazole-4,9-dione (7a). White solid (51% yield). ^{1}H NMR (400 MHz, DMSO-d_6) δ 9.29 (d, J = 10.4 Hz,

3H), 8.26 (s, 1H), 8.14 (d, J = 8.0 Hz, 3H), 8.01 (d, J = 8.4 Hz, 4H). ^{13}C NMR (101 MHz, DMSO-d_6) δ 177.10, 173.97, 160.35, 157.90, 145.01, 137.26, 135.00, 134.72, 133.36, 132.75, 130.92, 130.45, 129.59, 127.05, 125.18, 116.39, 116.17. HRMS m/z (ESI) calcd for $C_{20}H_{11}N_5O_2$ [M + Na]$^+$ 376.0913; found, 376.0811.

1-[4-(2-Methylpyridin-4-yl)phenyl]-1H,4H,9H-naphtho[2,3-d][1,2,3]triazole-4,9-dione (7b). White solid (34% yield). ^{1}H NMR (400 MHz, CDCl$_3$) δ 8.63 (d, J = 4.2 Hz, 1H), 8.39 (dd, J =6.4, 1.6 Hz, 1H), 8.24 (dd, J = 6.4, 1.2 Hz, 1H), 7.92–7.82 (m, 6H), 7.45 (s, 1H), 7.39 (d, J = 4.8 Hz, 1H), 2.67 (s, 3H). ^{13}C NMR (101 MHz, CDCl$_3$) δ 176.86, 174.37, 159.33, 149.90, 147.02, 146.05, 141.10, 135.61, 135.42, 135.30, 134.58, 133.36, 133.13, 133.04, 127.94, 127.81, 127.70, 127.55, 125.66, 121.30, 118.91, 24.62. HRMS m/z (ESI) calcd for $C_{23}H_{15}N_3O_3$ [M + Na]$^+$ 389.1117; found, 389.1028.

1-{2'-Hydroxy-[1,1'-biphenyl]-4-yl}-1H,4H,9H-naphtho[2,3-d][1,2,3]triazole-4,9-dione (7c). White solid (31% yield). ^{1}H NMR (400 MHz, DMSO-d_6) δ 9.79 (s, 1H), 8.29–8.22 (m, 1H), 8.14 (dd, J = 5.6, 1.6 Hz, 1H), 8.04–7.92 (m, 2H), 7.83 (s, 4H), 7.40 (dd, J = 6.4, 1.2 Hz, 1H), 7.24 (s, 1H), 7.02(d, J = 8.0 Hz, 1H) ,6.99 (t, J = 7.2 Hz, 1H).^{13}C NMR (101 MHz, DMSO-d_6) δ 177.11, 173.95, 154.48, 145.02, 140.87, 134.95, 134.68, 134.51, 133.56, 133.37, 132.77, 130.41, 129.67, 129.31, 127.03, 126.84, 126.27, 124.88, 119.63, 116.21.HRMS m/z (ESI) calcd for $C_{22}H_{13}N_3O_3$ [M + H]$^+$368.0957; found, 368.1044; [M + Na]$^+$390.0957; found,390.0858.

1-{3'-Hydroxy-[1,1'-biphenyl]-4-yl}-1H,4H,9H-naphtho[2,3-d][1,2,3]triazole-4,9-dione(7d) . White solid (21% yield). ^{1}H NMR (400 MHz, DMSO-d_6) δ 10.17–9.37 (m, 1H), 8.26 (d, J = 8.8 Hz, 1H), 8.15 (d, J = 6.8 Hz, 1H), 7.96 (d, J = 5.6 Hz, 2H), 7.89 (s, 4H), 7.33 (t, J = 7.6 Hz, 1H), 7.24–7.10 (m, 2H), 6.86 (dd, J = 6.4, 1.6 Hz, 1H).^{13}C NMR (101 MHz, DMSO-d_6) δ 177.12, 173.98, 158.03, 145.01, 142.45, 140.18, 134.97, 134.70, 134.60, 134.37, 133.38, 132.76, 130.16, 127.26, 127.04, 126.85, 125.80, 117.70, 115.27, 113.77.HRMS m/z (ESI) calcd for $C_{22}H_{13}N_3O_3$ [M + H]$^+$ 367.0957; found, 367.1184; [M + Na]$^+$ 389.0957; found, 389.1017.

1-{4'-Amino-[1,1'-biphenyl]-4-yl}-1H,4H,9H-naphtho[2,3-d][1,2,3]triazole-4,9-dione (7e). White solid (29% yield). ^{1}H NMR (400 MHz, DMSO-d_6) δ 8.24 (d, J =

6.8Hz, 1H), 8.14 (d, J = 6.0 Hz, 1H), 7.96 (t, J = 5.6 Hz, 2H), 7.80 (q, J = 8.7 Hz, 4H), 7.52 (d, J = 8.4 Hz, 2H), 6.70 (d, J = 8.4 Hz, 2H), 5.39 (s, 2H). ^{13}C NMR (101 MHz, DMSO-d_6) δ 177.12, 173.98, 158.03, 145.01, 142.45, 140.18, 134.97, 134.70, 134.60, 134.37, 133.38, 132.76, 130.16, 127.26, 127.04, 126.85, 125.80, 117.70, 115.27, 113.77. HRMS m/z (ESI) calcd for $C_{22}H_{14}N_4O_2$ [M + H]$^+$ 367.1117; found,367.1194; [M + Na]$^+$ 389.1117; found,389.1017.

1-{3'-Amino-[1,1'-biphenyl]-4-yl}-1H,4H,9H-naphtho[2,3-d][1,2,3]triazole-4,9-dione (7f). White solid (31% yield). ^{1}H NMR (400 MHz, DMSO-d_6) δ 8.25 (d, J = 8.4 Hz, 1H), 8.14 (s, 1H), 7.96 (s, 2H), 7.85 (dd, J = 8.4, 8.4 Hz, 4H), 7.17 (t, J = 7.6Hz, 1H), 6.99 (s, 1H) 6.88 (d, J = 7.6 Hz 1H), 6.65 (d, J = 7.6 Hz, 1H), 5.25 (s, 2H). ^{13}C NMR (101 MHz, DMSO-d_6) δ 177.61, 174.47, 149.79, 145.50, 143.73, 139.98, 135.45, 135.17, 135.06, 134.61, 133.88, 133.26, 130.11, 127.52, 127.33, 126.19, 115.01, 114.37, 112.71.HRMS m/z (ESI) calcd for $C_{22}H_{14}N_4O_2$ [M + H]$^+$ 367.1117; found,367.1201; [M + Na]$^+$ 389.1117; found, 389.1015.

1-{2'-Amino-[1,1'-biphenyl]-4-yl}-1H,4H,9H-naphtho[2,3-d][1,2,3]triazole-4,9-dione (7g). White solid (19% yield). ^{1}H NMR (400 MHz, DMSO-d_6) δ 8.28–8.22 (m, 1H), 8.15 (d, J = 6.4 Hz, 1H), 7.95 (m, 2H), 7.89 (d, J = 8.4 Hz, 2H), 7.72 (d, J = 8.4 Hz, 2H), 7.11 (t, J = 7.6 Hz, 2H), 6.83 (d, J = 7.6 Hz, 1H), 6.70 (t, J = 7.2 Hz, 1H), 4.96 (s, 2H). ^{13}C NMR (101 MHz, DMSO-d_6) δ 177.60, 174.43, 145.69, 145.51, 142.59, 135.44, 135.18, 135.00, 134.20, 133.87, 133.24, 130.68, 129.78, 129.33, 127.53, 127.32, 126.09, 124.78, 117.41, 116.13.HRMS m/z (ESI) calcd for $C_{22}H_{14}N_4O_2$ [M + H]$^+$ 367.1117; found, 367.1189; [M + Na]$^+$ 389.1117; found, 389.1019.

1-{2'-Fluoro-[1,1'-biphenyl]-4-yl}-1H,4H,9H-naphtho[2,3-d][1,2,3]triazole-4,9-dione (11a). White solid (31% yield). ^{1}H NMR (400 MHz, DMSO-d_6) δ 8.26 (d, J = 6.9 Hz, 1H), 8.15 (d, J = 6.6 Hz, 1H), 8.03–7.92 (m, 4H), 7.85 (d, J = 7.9 Hz, 2H), 7.69 (t, J = 7.6 Hz, 1H), 7.55–7.48 (m, 1H), 7.40 (dd, J = 14.8, 7.6 Hz, 2H). ^{13}C NMR (101 MHz, DMSO-d_6) δ 177.10, 173.97, 160.35, 157.90, 145.01, 137.26, 135.00 (d, J = 8.08 Hz), 134.70 (d, J = 5.05 Hz), 133.35, 132.73, 131.12 (d, J = 9.09 Hz), 127.57, 127.04, 126.85, 125.89, 123.13 (d, J = 3.03 Hz), 115.09, 114.88, 113.92 (d, J = 22.22 Hz).HRMS m/z (ESI) calcd for $C_{22}H_{12}FN_3O_2$ [M + Na]$^+$ 392.0914; found, 392.0806.

1-{3'-Fluoro-[1,1'-biphenyl]-4-yl}-1*H*,4*H*,9*H*-naphtho[2,3-*d*][1,2,3]triazole-4,9-dione (11b). White solid (43% yield). ^{1}H NMR (400 MHz, DMSO-d_6) δ 8.26 (dd, J = 6.4, 2.0 Hz, 1H), 8.15 (d, J = 6.4 Hz, 1H), 8.08–7.89 (m, 6H), 7.70 (ddd, J = 5.6, 2.4, 1.6 Hz, 2H), 7.59 (td, J = 6.0, 2.4 Hz, 1H), 7.29 (ddd, J = 5.6, 1.6, 0.8 Hz, 1H).^{13}C NMR (101 MHz, DMSO-d_6) δ 177.08, 173.96, 163.94, 161.52, 144.99, 141.17, 141.10, 140.79, 140.77, 134.98 (d, J = 8.08 Hz), 134.70 (d, J = 5.05 Hz), 133.35, 132.73, 131.12 (d, J = 9.09 Hz), 127.57, 127.04, 126.85, 125.89, 123.13 (d, J = 3.03 Hz), 115.09, 114.88, 113.92 (d, J = 22.22 Hz).HRMS m/z (ESI) calcd for $C_{22}H_{12}FN_3O_2$ [M + H]$^+$ 370.0914; found, 370.0989; [M + Na]$^+$ 392.0914; found, 392.0805.

Methyl-4'-{4,9-dioxo-1*H*,4*H*,9*H*-naphtho[2,3-*d*][1,2,3]triazol-1-yl}[1,1'-biphenyl]-3-carboxylate (11c). White solid (21% yield). ^{1}H NMR (400 MHz, DMSO-d_6) δ 8.33 (s, 1H), 8.26 (d, J = 7.6 Hz, 1H), 8.13 (dd, J = 7.6, 5.6 Hz, 2H), 8.07–7.91 (m, 7H), 7.72 (t, J = 8.4 Hz, 1H), 3.92 (s, 3H).^{13}C NMR (101 MHz, DMSO-d_6) δ 177.60, 166.54, 139.80, 135.20, 133.26, 132.35, 131.04, 130.24, 128.12, 127.95, 127.54, 126.52, 52.83.HRMS m/z (ESI) calcd for $C_{24}H_{15}N_3O_4$ [M + H]$^+$ 410.1063; found,410.1144; [M + Na]$^+$ 432.1063; found, 432.0959.

1-{3',4',5'-Trimethoxy-[1,1'-biphenyl]-4-yl}-1*H*,4*H*,9*H*-naphtho[2,3-*d*][1,2,3]triazole-4,9-dione (11d). White solid (28% yield). ^{1}H NMR (400 MHz, DMSO-d_6) δ 8.26 (d, J = 8.8 Hz, 1H), 8.14 (s, 1H), 7.99 (d, J = 8.8 Hz, 4H), 7.89 (d, J = 8.0 Hz, 2H), 7.07 (s, 2H), 3.91 (s, 6H), 3.73 (s,3H). NMR (101 MHz, DMSO-d_6) δ 177.59, 174.45, 153.83, 145.49, 142.89, 138.25, 135.45, 135.18, 134.95, 134.75, 133.87, 133.25, 127.92, 127.53, 127.35, 126.14, 105.07, 60.58, 56.55. HRMS m/z (ESI) calcd for $C_{25}H_{19}N_3O_5$ [M + H]$^+$ 441.1325; found, 442.1395; [M + Na]$^+$ 464.1325; found, 464.1216.

1-{2-Methoxy-[1,1'-biphenyl]-4-yl}-1*H*,4*H*,9*H*-naphtho[2,3-*d*][1,2,3]triazole-4,9-dione (11e). White solid (36% yield). ^{1}H NMR (400 MHz, CDCl$_3$) δ 8.40 (dd, J = 6.4, 1.2 Hz, 1H), 8.25 (dd, J = 6.4, 1.2 Hz, 1H), 7.86 (dtd, J = 18.6, 6.0, 1.4 Hz, 2H), 7.62–7.57 (m, 2H), 7.53 (d, J = 8.0 Hz, 1H), 7.49–7.37 (m, 5H), 3.91 (s, 3H). ^{13}C NMR (101 MHz, CDCl$_3$) δ 177.59, 174.38, 156.73, 145.40, 137.38, 135.88, 135.45, 135.21, 133.90,

133.18, 132.37, 131.21, 129.81, 128.68, 128.02, 127.62, 127.34, 118.02, 109.91, 56.63. HRMS m/z (ESI) calcd for $C_{23}H_{15}N_3O_3$ [M + Na]$^+$ 404.1113; found, 404.1002.

1-{3'-Methoxy-[1,1'-biphenyl]-4-yl}-1*H*,4*H*,9*H*-naphtho[2,3-*d*][1,2,3]triazole-4,9-dione (11f) . White solid (17% yield). ^{1}H NMR (400 MHz, DMSO-d_6) δ 8.28–8.23 (m, 1H), 8.16–8.13 (m, 1H), 7.98 (d, J = 8.8 Hz, 4H), 7.90 (d, J = 8.8 Hz, 2H), 7.46 (t, J = 8.0 Hz, 1H), 7.41 – 7.33 (m, 2H), 7.03 (dd, J = 8.0, 2.0 Hz, 1H), 3.87 (s, 3H).^{13}C NMR (101 MHz, DMSO-d_6) δ 177.12, 173.97, 159.86, 145.01, 142.15, 140.24, 134.98, 134.71, 134.63, 134.53, 133.38, 132.76, 130.21, 127.49, 127.05, 126.86, 125.80, 119.30, 113.95, 112.46, 99.51, 55.23.HRMS m/z (ESI) calcd for $C_{23}H_{15}N_3O_3$ [M + Na]$^+$ 404.1113; found, 404.0972.

1-[3',5'-Bis(trifluoromethyl)-[1,1'-biphenyl]-4-yl]-1*H*,4*H*,9*H*-naphtho[2,3-*d*][1,2,3]triazole-4,9-dione (11g). White solid (28% yield). ^{1}H NMR (400 MHz, CDCl$_3$) δ 8.40 (dd, J = 6.4, 1.2 Hz, 1H), 8.25 (dd, J = 6.4, 1.2 Hz, 1H), 8.11 (s, 2H), 7.96–7.83 (m, 7H). ^{13}C NMR (101 MHz, CDCl$_3$) δ 176.84, 174.39, 146.10, 141.64, 140.70, 135.70, 135.35, 134.61, 133.40, 133.11 (d, J = 6.06 Hz), 132.73, 132.40, 128.18, 127.85 (d, J = 12.12 Hz,), 127.43, 125.93, 121.86. HRMS m/z (ESI) calcd for $C_{24}H_{11}F_6N_3O_2$ [M + H]$^+$ 488.0755; found,488.0836. [M + Na]$^+$ 510.0755; found, 488.0644.

1-[3-Fluoro-4'-(propan-2-yl)-[1,1'-biphenyl]-4-yl]-1*H*,4*H*,9*H*-naphtho[2,3-*d*][1,2,3]triazole-4,9-dione (11h). White solid (37% yield). ^{1}H NMR (400 MHz, CDCl$_3$) δ 8.40 (dd, J = 7.6, 1.2 Hz, 1H), 8.22 (dd, J = 7.6, 1.2 Hz, 1H), 7.88 (td, J = 7.2, 1.2 Hz, 1H), 7.83 (td, J = 7.2, 1.2 Hz, 1H), 7.71 (t, J = 7.6 Hz, 1H), 7.63–7.55 (m, 4H), 7.38 (d, J = 8.0 Hz, 2H),3.00 (dt, J = 13.6, 6.8 Hz, 1H), 1.32 (d, J = 6.8 Hz, 6H).^{13}C NMR (101 MHz, CDCl$_3$) δ 176.90, 174.25, 157.57, 155.04, 150.03, 146.60 (d, J = 7.07 Hz), 145.39, 136.01(d, J = 1.01 Hz), 135.35, 134.76, 134.61, 133.39, 133.05, 127.98, 127.78, 127.62, 127.42, 127.32, 123.33 (d, J = 3.03 Hz), 122.32 (d, J = 13.13 Hz), 115.20 (d, J = 19.19 Hz), 34.02, 29.82, 24.03.HRMS m/z (ESI) calcd for $C_{25}H_{18}FN_3O_2$ [M + Na]$^+$ 434.1383; found, 434.1126.

1-[3,5-Difluoro-4'-(propan-2-yl)-[1,1'-biphenyl]-4-yl]-1*H*,4*H*,9*H*-naphtho[2,3-*d*][1,2,3]triazole-4,9-dione (11i). White solid (28% yield). ^{1}H NMR (400 MHz, CDCl$_3$) δ 8.41 (dd, J = 7.6, 1.2 Hz, 1H), 8.20 (dd, J = 7.6, 1.2 Hz, 1H), 7.89 (td, J = 7.5, 1.3 Hz,

1H), 7.83 (td, J = 7.2, 1.2 Hz, 1H), 7.58 (d, J = 8.4 Hz, 2H), 7.40 (t, J = 8.4 Hz, 4H),

3.00 (dt, J = 13.6, 6.8 Hz, 1H), 1.32 (d, J = 6.9 Hz, 6H). ^{13}C NMR (101 MHz, CDCl$_3$)

δ 176.79, 174.13, 157.46, 154.93, 149.92, 146.49 (d, J = 8.08 Hz), 145.28, 135.89 (d, J

= 1.01 Hz), 135.24, 134.64, 134.49, 133.28, 132.94, 127.86, 127.67, 127.51, 127.31,

127.20, 123.22 (d, J = 4.04 Hz), 122.21 (d, J = 13.13 Hz), 115.08 (d, J = 19.19 Hz),

33.90, 29.70, 23.92.HRMS m/z (ESI) calcd for

C$_{25}$H$_{17}$F$_2$N$_3$O$_2$[M+Na]$^+$452.1289;found,452.1157.

1-[2,6-Difluoro-4'-(propan-2-yl)-[1,1'-biphenyl]-4-yl]-1H,4H,9H-naphtho[2,3-

d][1,2,3]triazole-4,9-dione (11j). White solid (19% yield). ^{1}H NMR (400 MHz,

DMSO-d_6) δ 8.27 (d, J = 8.8 Hz, 1H), 8.18 (s, 1H), 7.99 (s, 2H), 7.86 (d, J = 5.6Hz,

2H), 7.52 (d, J = 8.0 Hz, 2H), 7.45 (d, J = 8.4 Hz, 2H), 2.99 (dt, J = 13.6, 6.8 Hz, 1H),

1.28 (d, J = 6.8 Hz, 6H). ^{13}C NMR (101 MHz, DMSO-d_6) δ 177.39, 174.34, 160.64 (d,

J= 9.09 Hz), 160.55, 158.18 (d, J= 9.09 Hz), 149.94, 145.30, 135.66 (d, J= 19.19 Hz),

133.72, 133.09, 130.56, 127.69, 127.44, 127.14, 126.28, 125.24, 120.51, 110.70 (d, J=

31.31 Hz), 33.79, 24.22. HRMS m/z (ESI) calcd for C$_{25}$H$_{17}$F$_2$N$_3$O$_2$ [M + H]$^+$ 430.1289;

found, 430.1359; [M + Na]$^+$ 452.1289; found, 430.1186.

1-{2,6-Difluoro-3'-methoxy-[1,1'-biphenyl]-4-yl}-1H,4H,9H-naphtho[2,3-

d][1,2,3]triazole-4,9-dione (11k). White solid (35% yield). ^{1}H NMR (400 MHz, CDCl$_3$)

δ 8.39 (dd, J = 6.0, 1.6 Hz, 1H), 8.27 (dd, J = 7.2, 1.2 Hz, 1H), 7.88 (dqd, J = 14.8, 7.2,

1.4 Hz, 2H), 7.58–7.52 (m, 2H), 7.44 (t, J = 7.6 Hz, 1H), 7.12 (d, J = 7.6 Hz, 1H), 7.07

(s, 1H), 7.05–7.00 (m, 1H), 3.88 (s, 3H). ^{13}C NMR (101 MHz, CDCl$_3$) δ 176.80, 174.38,

161.23 (d, J= 8.08 Hz), 159.72, 158.73(d, J= 8.08 Hz), 146.24, 135.61, 135.04, 134.86,

133.52, 133.15, 133.02, 129.71, 128.94, 127.99, 122.72, 121.20 (d, J= 19.19 Hz),

115.97, 114.89, 109.53 (d, J=31.31 Hz), 109.43 (d, J=11.11 Hz), 55.53. HRMS m/z

(ESI) calcd for C$_{23}$H$_{13}$F$_2$N$_3$O$_3$ [M + H]$^+$ 418.0925; found, 418.0991; [M + Na]$^+$

440.0925; found, 440.0814.

1-{2,2',6-Trifluoro-[1,1'-biphenyl]-4-yl}-1H,4H,9H-naphtho[2,3-d][1,2,3]triazole-

4,9-dione (11l). White solid (39% yield). ^{1}H NMR (400 MHz, CDCl$_3$) δ 8.39 (dt, J =

4.6, 2.5 Hz, 1H), 8.31–8.24 (m, 1H), 7.89 (dqd, J = 14.6, 7.4, 1.4 Hz, 2H), 7.62–7.54

(m, 2H), 7.54 –7.44 (m, 2H), 7.34–7.27 (m, 1H), 7.25 (d, J = 9.0 Hz, 1H). ^{13}C NMR

(101 MHz, CDCl$_3$) δ 176.64, 174.19, 161.23 (d, J= 248.46 Hz), 161.01(d, J= 8.08 Hz) 158.51(d, J= 8.08 Hz), 146.13, 135.84, 134.72, 133.37, 133.00, 132.85, 132.02, 131.41 (d, J= 8.08 Hz), 127.87, 127.85, 124.20, 124.16, 116.17 (d, J= 22.22 Hz), 115.95 (d, J= 16.16 Hz), 115.63 (d, J=20.20 Hz), 109.17 (d, J= 31.31 Hz), 109.07 (d, J= 12.12 Hz). HRMS m/z (ESI) calcd for C$_{22}$H$_{10}$F$_3$N$_3$O$_2$ [M + H]$^+$ 406.0725; found,406.0801; [M + Na]$^+$ 428.0725; found,428.0631.

1-{2,3',6-Trifluoro-[1,1'-biphenyl]-4-yl}-1H,4H,9H-naphtho[2,3-d][1,2,3]triazole-4,9-dione (11m). White solid (18% yield). ^{1}H NMR (400 MHz, DMSO-d_6) δ 8.29–8.25 (m, 1H), 8.19 (dd, J = 5.2, 1.6 Hz, 1H), 8.04–7.96 (m, 2H), 7.90 (d, J = 7.6 Hz, 2H), 7.66–7.60 (m, 1H), 7.53 (d, J = 9.6 Hz, 1H), 7.46 (d, J = 7.6 Hz, 1H), 7.39 (ddd, J = 2.8, 2.4,1.6 Hz, 1H). ^{13}C NMR (101 MHz, DMSO-d_6) δ 177.39, 174.34, 163.68, 161.26, 158.06, 145.32, 136.16, 135.68, 135.51, 135.36, 133.71, 133.08, 131.25 (d, J = 8.08 Hz), 127.70, 127.45, 126.94, 117.75 (d, J = 20.2 Hz), 116.68 (d, J = 20.2 Hz), 110.76 (d, J = 31.31 Hz).HRMS m/z (ESI) calcd for C$_{22}$H$_{10}$F$_3$N$_3$O$_2$ [M + Na]$^+$ 428.0725; found, 428.0613.

1-{2,4',6-Trifluoro-[1,1'-biphenyl]-4-yl}-1H,4H,9H-naphtho[2,3-d][1,2,3]triazole-4,9-dione (11n). White solid (25% yield). ^{1}H NMR (400 MHz, DMSO-d_6) δ 8.22 (m , 2H), 8.05–7.82 (m, 4H), 7.65 (s, 4H). ^{13}C NMR (101 MHz, DMSO-d_6) δ 177.39, 174.34, 163.68, 161.26, 158.06, 145.32, 136.16, 135.68, 133.71, 133.08, 131.27 (d, J = 8.08 Hz), 131.17, 127.70, 127.45, 126.94, 116.68, 116.48, 110.86 (d, J = 31.31 Hz). HRMS m/z (ESI) calcd for C$_{22}$H$_{10}$F$_3$N$_3$O$_2$ [M + Ka]$^+$ 444.0725; found, 444.0364.

1-[2,6-Difluoro-3'-(hydroxymethyl)-[1,1'-biphenyl]-4-yl]-1H,4H,9H-naphtho[2,3-d][1,2,3]triazole-4,9-dione (11o). White solid (21% yield). ^{1}H NMR (400 MHz, DMSO-d_6) δ 8.31–8.25 (m, 1H), 8.21–8.17 (m, 1H), 8.05–7.95 (m, 2H), 7.92–7.85 (m, 2H), 7.59–7.50 (m, 2H), 7.49–7.44 (m, 2H), 5.34 (t, J = 5.6 Hz, 1H), 4.60 (d, J = 6.4 Hz, 2H). ^{13}C NMR (101 MHz, DMSO-d_6) δ 176.91, 173.87, 160.11 (d, J = 8.08 Hz), 157.65 (d, J = 8.08 Hz), 144.84, 143.14, 135.33, 135.18, 134.99, 134.87, 133.23, 132.59, 128.46, 128.40, 127.95, 127.21 (d, J = 4.04 Hz), 126.96, 120.37 (d, J = 19.19 Hz), 110.22 (d, J = 31.31 Hz), 62.58,28.29. HRMS m/z (ESI) calcd for C$_{23}$H$_{13}$F$_2$N$_3$O$_3$ [M + Na]$^+$ 440.0925; found, 440.0833.

1-[2,6-Difluoro-3'-(methoxymethyl)-[1,1'-biphenyl]-4-yl]-1*H*,4*H*,9*H*-naphtho[2,3-*d*][1,2,3]triazole-4,9-dione (11p). White solid (27% yield). ^{1}H NMR (400 MHz, DMSO-d_6) δ 8.27 (dd, J = 5.2, 2.4 Hz, 1H), 8.22–8.16 (m, 1H), 8.04–7.95 (m, 2H), 7.88 (d, J = 8.0 Hz, 2H), 7.54 (dd, J = 7.2, 7.2 Hz, 3H), 7.47 (d, J = 7.2 Hz, 1H), 4.52 (s, 2H), 3.35 (s, 3H). ^{13}C NMR (101 MHz, DMSO-d_6) δ 176.91, 173.87, 160.11 (d, J = 8.08 Hz), 157.65 (d, J = 8.08 Hz), 144.84, 143.14, 135.33, 135.18, 134.99, 134.87, 133.23, 132.59, 128.46, 128.40, 127.95, 127.21 (d, J = 4.04 Hz), 126.96, 120.37 (d, J = 19.19 Hz), 110.22 (d, J = 31.31 Hz), 62.58, 28.29, 22.56. HRMS m/z (ESI) calcd for $C_{24}H_{15}F_2N_3O_3$ (ESI): [M + Na]$^+$ 454.1081; found, 454.0971; [M + H]$^+$ 432.1081; found, 432.1141.

Methyl-2-(4'-{4,9-dioxo-1*H*,4*H*,9*H*-naphtho[2,3-*d*][1,2,3]triazol-1-yl}-2',6'-difluoro-[1,1'-biphenyl]-3-yl)acetate (11q). White solid (29% yield). ^{1}H NMR (400 MHz, DMSO-d_6) δ 8.29–8.26 (m, 1H), 8.20–8.18 (m, 1H), 8.03–7.96 (m, 2H), 7.88 (d, J = 8.0 Hz, 2H), 7.56–7.48 (m, 3H), 7.43 (d, J = 7.6 Hz, 1H), 3.81 (s, 2H), 3.65 (s, 3H). ^{13}C NMR (101 MHz, DMSO) δ 177.39, 174.35, 171.95, 160.56 (d, J = 8.08 Hz), 158.10 (d, J = 8.08 Hz), 145.32, 135.66, 135.46, 135.41, 135.35, 133.70, 133.07, 131.49, 130.68, 129.21 (d, J = 11.11 Hz), 127.88, 127.69, 127.44, 120.31 (d, J = 20.2 Hz), 110.73, 110.42, 56.50, 52.26, 49.07, 19.00. HRMS m/z (ESI) calcd for $C_{25}H_{15}F_2N_3O_4$ [M + H]$^+$ 472.1031; found, 472.0846.

1-[3'-(Dimethylamino)-2,6-difluoro-[1,1'-biphenyl]-4-yl]-1*H*,4*H*,9*H*-naphtho[2,3-*d*][1,2,3]triazole-4,9-dione (11r). White solid (17% yield). ^{1}H NMR (400 MHz, DMSO-d_6) δ 8.29–8.25 (m, 1H), 8.21–8.16 (m, 1H), 8.04–7.95 (m, 2H), 7.84 (d, J = 7.6 Hz, 2H), 7.35 (dd, J = 7.6, 1.6 Hz, 1H), 6.86 (d, J = 5.6 Hz, 2H), 6.81 (d, J = 7.6 Hz, 1H), 2.95 (s, 6H). ^{13}C NMR (101 MHz, DMSO-d_6) δ 177.41, 174.35, 150.92, 145.21, 135.71, 135.66, 135.66, 135.46 (d, J = 11.11 Hz), 133.72, 133.09, 129.64, 129.64, 128.43, 127.68, 127.68, 127.44, 118.04, 114.38, 114.17, 113.37, 110.61, 108.18, 72.90, 24.92, 18.85. HRMS m/z (ESI) calcd for $C_{24}H_{16}F_2N_4O_2$ [M + H]$^+$ 431.1241; found, 431.1321.

1-[2,2',6-Trifluoro-5'-(hydroxymethyl)-[1,1'-biphenyl]-4-yl]-1*H*,4*H*,9*H*-naphtho[2,3-*d*][1,2,3]triazole-4,9-dione (11s). White solid (31% yield). ^{1}H NMR (400

MHz, DMSO-d_6) δ 8.30–7.87 (m, 6H), 7.55 (d, J = 6.4 Hz, 2H), 7.43 (t, J = 9.6 Hz, 1H), 5.36 (t, J = 5.2Hz, 1H), 4.58 (d, J = 4.4 Hz, 2H). ^{13}C NMR (101 MHz, DMSO-d_6) δ 176.91, 173.87, 160.11(d, J = 8.08 Hz), 157.65(d, J = 8.08 Hz), 144.84, 143.14, 135.33, 135.18, 134.99, 134.87, 133.23, 132.59, 128.46 (d, J = 6.06 Hz), 127.95, 127.21 (d, J = 4.04 Hz), 126.96, 120.37 (d, J = 19.19 Hz), 110.22 (d, J = 31.31 Hz). HRMS m/z (ESI) calcd for $C_{23}H_{12}F_3N_3O_3$ [M + Na]$^+$ 458.0831; found, 458.0697.

6-Methoxy-1-{2,2',6-trifluoro-[1,1'-biphenyl]-4-yl}-1H,4H,9H-naphtho[2,3-d][1,2,3]triazole-4,9-dione (14a). Yellow solid (29% yield). ^{1}H NMR (400 MHz, CDCl$_3$) δ 8.36–8.31 (m, 1H), 7.69 (d, J = 1.2 Hz, 1H), 7.62–7.54 (m, 2H), 7.49 (ddd, J = 7.0, 3.6, 2.0 Hz, 2H), 7.36–7.27 (m, 3H), 3.99 (s, 3H).^{13}C NMR (101 MHz, CDCl$_3$) δ 175.85, 174.20, 164.78, 161.24, 158.76(d, J=8.08 Hz), 158.71(d, J=8.08 Hz), 146.40, 135.15, 133.33, 131.41, 131.33, 130.27, 126.09, 124.21, 124.17, 121.07, 116.17(d, J=22.22 Hz), 115.95(d, J=16.16 Hz), 115.66(d, J=20.20 Hz), 115.50, 111.95(d, J=31.31 Hz), 108.81(d, J=12.12 Hz), 56.13.HRMS m/z (ESI) calcd for $C_{23}H_{12}F_3N_3O_3$ [M + Na]$^+$436.0831; found,436.0888.

7-Methoxy-1-{2,2',6-trifluoro-[1,1'-biphenyl]-4-yl}-1H,4H,9H-naphtho[2,3-d][1,2,3]triazole-4,9-dione (14b). Yellow solid (31% yield). ^{1}H NMR (400 MHz, DMSO-d_6) δ 8.21–8.08 (m, 1H), 7.93 (s, 2H), 7.68 (dd, J =7.6, 7.2 Hz, 3H), 7.54–7.40 (m, 3H), 4.02 (s, 3H).^{13}C NMR (101 MHz, DMSO-d_6) δ 177.60, 174.46, 160.34, 145.49, 142.63(d, J = 8.08 Hz), 140.73(d, J=8.08 Hz Hz), 135.47, 135.19, 135.12, 135.02, 133.86, 133.24, 130.69, 127.98, 127.53(d, J=22.22 Hz), 127.34(d, J=16.16 Hz), 126.28(d, J=20.20 Hz), 119.78, 114.43(d, J=31.31 Hz), 112.94(d, J=12.12 Hz), 55.72.HRMS m/z (ESI) calcd for $C_{23}H_{12}F_3N_3O_3$ [M + Na]$^+$436.0831; found,436.0888.

6-Hydroxy-1-{2,2',6-trifluoro-[1,1'-biphenyl]-4-yl}-1H,4H,9H-naphtho[2,3-d][1,2,3]triazole-4,9-dione (14c). White solid (67% yield). ^{1}H NMR (400 MHz, DMSO-d_6) δ 11.32 (s, 1H), 8.06 (d, J = 8.4 Hz, 1H), 7.91 (d, J = 7.6 Hz, 2H), 7.64 (dd, J = 6.4, 4.2 Hz, 2H), 7.56 (d, J = 2.4 Hz, 1H), 7.51–7.41 (m, 2H), 7.27 (dd, J = 9.0, 2.8 Hz, 1H). HRMS m/z (ESI) calcd for $C_{22}H_{10}F_3N_3O_3$ [M + Na]$^+$444.0831; found, 444.0533.

7-Hydroxy-1-{2,2',6-trifluoro-[1,1'-biphenyl]-4-yl}-1H,4H,9H-naphtho[2,3-

***d*][1,2,3]triazole-4,9-dione (14d).** White solid (64% yield). ^{1}H NMR (400 MHz, DMSO-d_6) δ 11.32 (s, 1H), 8.06 (d, J = 8.4 Hz, 1H), 7.91 (d, J = 7.6 Hz, 2H), 7.64 (dd, J = 6.4, 4.2 Hz, 2H), 7.56 (d, J = 2.4 Hz, 1H), 7.51–7.41 (m, 2H), 7.27 (dd, J = 9.0, 2.8 Hz,1H). HRMS m/z (ESI) calcd for $C_{22}H_{10}F_3N_3O_3$ [M + Na]$^+$444.0831; found,444.0539.

6-Fluoro-1-{2,2',6-trifluoro-[1,1'-biphenyl]-4-yl}-1*H*,4*H*,9*H*-naphtho[2,3-*d*][1,2,3]triazole-4,9-dione (14e). White solid (32% yield). ^{1}H NMR (400 MHz, DMSO-d_6) δ 8.35 (dd, J = 4.2, 2.8 Hz, 1H), 7.93 (d, J = 8.0 Hz, 2H), 7.85 (td, J = 6.0, 2.4 Hz, 1H), 7.70–7.60 (m, 2H), 7.52–7.40 (m, 2H). ^{13}C NMR (101 MHz, DMSO-d_6) δ 176.22, 173.17, 167.46(d, J=8.08 Hz), 164.92(d, J=8.08 Hz), 160.98, 158.52, 158.32, 145.28, 136.81, 135.68, 132.81, 132.47, 130.93, 129.88, 125.37, 122.61, 122.39, 116.55, 116.34, 115.50, 114.51(d, J=24.24 Hz), 114.27, 110.57, 110.26(d, J=31.31 Hz). HRMS m/z (ESI) calcd for $C_{22}H_9F_4N_3O_2$ [M + Na]$^+$446.0631; found,446.0510.

7-Fluoro-1-{2,2',6-trifluoro-[1,1'-biphenyl]-4-yl}-1*H*,4*H*,9*H*-naphtho[2,3-*d*][1,2,3]triazole-4,9-dione (14f). White solid (25% yield). ^{1}H NMR (400 MHz, DMSO-d_6) δ 8.35 (dd, J = 4.2, 2.8 Hz, 1H), 7.93 (d, J = 8.0 Hz, 2H), 7.85 (td, J = 6.0, 2.4 Hz, 1H), 7.70 – 7.60 (m, 2H), 7.52 – 7.40 (m, 2H). ^{13}C NMR (101 MHz, DMSO-d_6) δ 176.22, 173.17, 167.46(d, J=8.08 Hz), 164.92(d, J=8.08 Hz), 160.98, 158.52, 158.32, 145.28, 136.81, 135.68, 132.81, 132.47, 130.93, 129.88, 125.37, 122.61, 122.39, 116.55, 116.34, 115.50, 114.51(d, J=24.24 Hz), 114.27, 110.57, 110.26(d, J=31.31 Hz). HRMS m/z (ESI) calcd for $C_{22}H_9F_4N_3O_2$ [M + Na]$^+$446.0631; found,446.0510.

6,6-Dimethyl-1-{2,2',6-trifluoro-[1,1'-biphenyl]-4-yl}-4,5,6,7-tetrahydro-1*H*-1,2,3-benzotriazol-4-one (14g). White solid (27% yield). ^{1}H NMR (400 MHz, CDCl$_3$) δ 7.53–7.46 (m, 1H), 7.42 (t, J = 7.2 Hz, 1H), 7.34 (d, J = 6.8 Hz, 1H), 7.32–7.21 (m, 1H), 3.01 (s, 2H), 2.58 (s, 2H), 1.20 (s, 6H).^{13}C NMR (101 MHz, CDCl$_3$) δ 189.88, 189.17, 161.88(d, J=248.46 Hz), 161.80(d, J=8.08 Hz), 161.21(d, J=8.08 Hz), 158.72, 143.24, 131.43, 124.22,115.47(d, J=22.22 Hz), 115.31(d, J=16.16 Hz), 114.22(d, J=20.20 Hz), 107.11(d, J=31.31 Hz), 107.01(d, J=12.12 Hz), 106.80, 52.29, 50.57, 35.71, 28.37. HRMS m/z (ESI) calcd for $C_{20}H_{16}F_3N_3O$ [M + Na]$^+$394.1245; found,

394.1147. [M + K]$^+$410.1245; found, 410.0889.

1-{2,2',6-Trifluoro-[1,1'-biphenyl]-4-yl}-4,5,6,7-tetrahydro-1H-1,2,3-benzotriazol-4-one (14h). White solid (22% yield). ^{1}H NMR (400 MHz, CDCl$_3$) δ 7.53–7.46 (m, 1H), 7.42 (t, J = 7.2 Hz, 1H), 7.26 (s, 1H), 7.26 (s, 5H), 3.16 (t, J = 6.1 Hz, 2H), 2.74–2.69 (m, 2H), 2.37–2.28 (m, 2H).^{13}C NMR (101 MHz, CDCl$_3$) δ 189.72, 161.80, 161.20 (d, J=248.46 Hz), 159.38(d, J=8.08 Hz), 158.72(d, J=8.08 Hz), 144.13, 142.73, 131.36, 124.21, 116.16(d, J=22.22 Hz), 115.94(d, J=16.16 Hz), 114.23(d, J=20.20 Hz), 107.06(d, J=31.31 Hz), 106.97(d, J=12.12 Hz), 106.76, 38.16, 23.15, 22.11. HRMS m/z (ESI) calcd for C$_{18}$H$_{12}$F$_3$N$_3$O [M + Na]$^+$366.0932; found, 366.0828. [M + K]$^+$382.0932; found, 382.0576.

6-(Propan-2-yl)-1-{2,2',6-trifluoro-[1,1'-biphenyl]-4-yl}-4,5,6,7-tetrahydro-1H-1,2,3-benzotriazol-4-one (14i). White solid (23% yield). ^{1}H NMR (400 MHz, CDCl$_3$) δ 7.42 (d, J = 6.4 Hz, 1H), 7.36 (t, J = 6.4 Hz, 1H), 7.31–7.14 (m, 5H), 3.09–2.98 (m, 1H), 2.82 (dd, J = 11.2,4.2 Hz, 1H), 2.69 (d, J = 12.8 Hz, 1H), 2.48–2.38 (m, 1H), 2.17 (s, 1H), 1.77 (dd, J = 6.4, 6.4 Hz, 1H), 0.97 (d, J = 6.8 Hz, 6H).^{13}C NMR (101 MHz, CDCl$_3$) δ 189.75, 161.89, 161.21(d, J=248.46 Hz), 159.29 (d, J=8.08 Hz), 158.73 (d, J=8.08 Hz), 144.28, 142.86, 131.45, 124.26, 116.17, 115.95(d, J=16.16 Hz), 115.48(d, J=20.20 Hz), 115.32(d, J=31.31 Hz), 114.28(d, J=12.12 Hz), 106.93, 42.65, 42.10, 31.74, 25.35, 19.66, 19.57. HRMS m/z (ESI) calcd for C$_{21}$H$_{18}$F$_3$N$_3$O [M + Na]$^+$408.1402; found, 408.1307.

1-{2,2',6-Trifluoro-[1,1'-biphenyl]-4-yl}-1H,4H,9H-naphtho[2,3-d][1,2,3]triazole-4,9-diol (14j). White solid (39% yield). ^{1}H NMR (400 MHz, DMSO-d_6) δ 7.99 (d, J = 8.4 Hz, 2H), 7.73 (d, J = 7.0 Hz, 1H), 7.67–7.57 (m, 3H), 7.49–7.38 (m, 4H), 6.33 (s, 2H), 6.11 (s, 1H), 5.80 (s, 1H). ^{13}C NMR (101 MHz, DMSO-d_6) δ 159.18, 157.67(d, J = 8.08 Hz), 147.25(d, J = 8.08 Hz), 138.95, 137.23, 134.23, 132.84, 129.62, 129.17, 128.53, 128.33(t, J = 4.04 Hz), 125.33(t, J = 19.19 Hz), 124.85, 116.53, 116.32, 115.11, 112.09, 107.95, 107.65, 62.04, 60.92. HRMS m/z (ESI) calcd for C$_{22}$H$_{11}$F$_2$N$_3$O$_2$ [M + Na]$^+$ 432.1038.0819; found,432.0939.

4-Benzoyl-1-{2,2',6-trifluoro-[1,1'-biphenyl]-4-yl}-1H-1,2,3-triazole (14k). White solid (46% yield). ^{1}H NMR (400 MHz, DMSO-d_6) δ 9.72 (s, 1H), 8.19 (dd, J = 6.2, 7.6

Hz, 4H), 7.81–7.34 (m, 7H).^{13}C NMR (101 MHz, DMSO-d_6) δ 185.39, 161.44, 159.06(d, J=8.08 Hz), 158.51(d, J=8.08 Hz), 147.65, 136.84, 134.05, 132.76, 132.38, 132.29, 130.44, 129.16, 129.01, 125.30, 116.50(d, J=22.22 Hz), 116.29, 115.59(d, J=20.20 Hz), 115.43 d, J=31.31 Hz), 105.49(d, J=12.12 Hz), 105.18. HRMS m/z (ESI) calcd for $C_{21}H_{12}F_3N_3O$ [M + Na]$^+$402.0932; found,402.0821.

4-Phenyl-1-{2,2',6-trifluoro-[1,1'-biphenyl]-4-yl}-1H-1,2,3-triazole (14l). White solid (41% yield). ^{1}H NMR (400 MHz, DMSO-d_6) δ 9.70 (s, 1H), 8.19 (dd, J = 6.2, 7.5 Hz, 4H), 7.81–7.34 (m, 7H). ^{13}C NMR (101 MHz, DMSO-d_6) δ 161.59, 160.97, 159.04(d, J=8.08 Hz), 158.51(d, J=8.08 Hz), 146.68, 138.04, 134.16, 132.74, 132.31, 129.25, 128.94, 126.53, 126.38, 125.26, 116.47(d, J=22.22 Hz), 116.26(d, J=16.16 Hz), 115.62(d, J=20.20 Hz), 115.46(d, J=31.31 Hz), 112.25, 104.68, 104.37.HRMS m/z (ESI) calcd for $C_{20}H_{12}F_3N_3$ [M + Na]$^+$374.0983; found,374.0864.

*h*DHODH inhibition Assays. *h*DHODH inhibition profiles were performed using hDHODH Inhibitor Profiler services provided by Shanghai ChemPartner Co., Ltd. (Shanghai, China). Briefly, the test compounds or DMSO, *h*DHODH, 2, 6-dichloroindophenol sodium salt (DCIP), and CoQ$_{10}$ in the assay buffer were incubated together for 30 min. The assay was started by the addition of dihydroorotate. The reduction in DCIP was measured by a microplate reader (BMG Labtech) at absorbance of 600 nm. IC$_{50}$ values were determined using GraphPad Prism 7.0.

Protein Preparation. *h*DHODH was cloned into a vector derived from pET-28a (+) (Novagen), which contains an N-terminal SUMO tag, and overexpressed in *Escherichia coli* strain Rosetta (DE3) (Novagen) at 18 °C for 18 h. The cells were harvested by centrifugation, and cell pellet was resuspended in binding buffer (50 mM Tris–HCl pH 7.5, 500 mM NaCl, 0.33% Thesit, 10% glycerol, 1 mM PMSF). The cells were lysed by an ultrahigh-pressure homogenizer (JNBIO) and centrifuged. The resultant supernatant was collected and loaded onto a Ni-NTA column pre-equilibrated with binding buffer. After washing with binding buffer supplemented with 20 mM imidazole to remove nonspecifically binding proteins, the target protein was eluted using binding buffer supplemented with 250 mM imidazole. The eluted target protein was collected and dialyzed against binding buffer with ULP1 protease (1:100) for 16 h at 8 °C to

remove the SUMO tag. The digested protein was then passed through a Ni–NTA column (GE Healthcare) to remove free SUMO tag, uncleaved protein and ULP1 protease. The flow-through was collected and further purified via gel filtration (Superdex 200 10/300 GL, GE Healthcare) in a buffer consisting of 50 mM HEPES, pH 7.5, 400 mM NaCl, 10% glycerol, 1 mM EDTA and 0.05% Thesit on an AKTA system (GE Healthcare). The purified proteins were concentrated to 20 mg ml^{-1} and stored at -80°C until use.

Cocrystallization of *h*DHODH and inhibitors. Purified *h*DHODH was incubated with 2 mM dihydroorotic acid (DHO), 40 mM N,N-dimethylundecylamine-N-oxide (C11DAO), 20.8 mM N,N-dimethyldecylamine-N-oxide (DDAO), and 5-folds small molecule inhibitor for 2 h at 4 °C. Crystals of *h*DHODH and inhibitor were grown using the hanging-drop vapor diffusion method at 20 °C in a buffer consisting of 0.1 M acetate pH 4.6, 1.8–2.0 M ammonium sulfate, 30%-35% glycerol. Cubic crystals appeared after a week.

Data Collection and Structure Determination. Crystals were fished directly from the growing drop and flash frozen in liquid nitrogen. Diffraction data were collected on beamline BL19U1 of the National Facility for Protein Science Shanghai (NFPS) at Shanghai Synchrotron Radiation Facility. The data collected were processed using the HKL-3000 program suite[57]. Details of the data collection and processing statistics are summarized in TableS1. Structures were determined by molecular replacement using the *h*DHODH structure (PDB ID: ID3G) as a search model. Structure refinement and model building were performed with PHENIX[58] and Coot[59]. All models were validated with MolProbity[60]. All structure figures were prepared with PyMOL (https://pymol.org).

Cell lines and cell culture. All of the cell lines including human melanoma cell line A375, human colorectal cancer cell line HCT116, human cervical carcinoma cell line Hela, Human lung carcinoma cell line A549, human breast adenocarcinoma cell line MCF-7, human Burkitt's lymphoma (B-cell) cell line Raji and Nalmawa, human chronic myelogenous leukemia cell K562 cells were obtained from American Type Culture Collection (ATCC; Manassas, VA, USA). The cells were cultured in the

designated medium containing 10% fetal bovine serum (FBS) (v/v) at 37 °C in a humidified 5% CO_2 incubator according to ATCC guidelines.

Cell viability assay. Cell viability was determined using MTT assay. The cells (2-10 × 10^3 cells per well) were seeded into 96-well plates. After incubation for 24 h, cells were treated with compounds (0-10 μM) for 48h. Then, 20 μL of MTT reagent (5 mg/mL) was added to each well, followed by 2-4 h incubation. For the adherent cells, the media and MTT were carefully aspirated, and formazan crystals were dissolved in 150 μL of 100% DMSO. For the suspended cells, 50 μL of 20% acidified SDS (w/v) was used to dissolve the oxidative product, followed by overnight incubation. Finally, the absorbance at 570 nm was read using a Microplate Reader 3550-UV (ThermoFisher Scientific). All experiments were performed in triplicate. The IC_{50} values were calculated using GraphPad Prism 7.0 software.

Cell Cycle and Apoptosis Assay. Cells (2 × 10^5 cells per well) were plated in a six-well plates and treated with compound 11k, 11l and BRQ for 24 or 48 h. After incubation, the cells were harvested and washed with ice-cold PBS. Cell cycle progression was analyzed using propidine iodide (PI) (50 mg/L, RNase free) staining. Cell apoptosis were detected by using Annexin V/FITC Apoptosis Detection Kit I (Keygen Tec, Nanjing, China) according to the manufacturer's instructions.

Detection of ROS. ROS level was detected using dihydroethidium (DHE, L1392, ThermoFisher Scientific), which measure the cellular superoxide. Briefly, after treatment with compound **11k**, **11l** and BRQ for 24h, cells were harvested and stained with 10 μM DHE dissolved in pre-warmed PBS for 15 min in dark. The fluorescence intensity of DHE was measured at 510 nm (excitation) and 600 nm (emission) using a Varioskan™ LUX multimode microplate reader (ThermoFisher Scientific) with SkanIt Software 5.0.

Mitochondrial membrane potential assay. Depletion of the mitochondrial membrane potential (Δψ) was determined by using the dye tetramethylrhodamine methyl ester (TMRM, Molecular Probes). The Raji cells were treated with compound **11l**, **11k**, BRQ and CCCP (positive control) for 48 h, followed by washing with PBS. Cells were harvested and incubated with TMRM at a final concentration of 100 nM for 15 min at

37 °C. The fluorescence intensity was detected at 510 nm (excitation) and 580 nm (emission) by a Varioskan™ LUX multimode microplate reader.

***In Vitro* physiological stability assay.** The physiological stability of compound **11l** and **11l-NC** and BRQ were determined by examining the stability of compounds in buffers with various pH values. The compounds with final concentration of 0.01 mg/mL were mixture with buffer containing 10% acetonitrile with pH values of 1.0, 4.5, 6.6, 7.4 or 9.0, respectively. After incubation at 37 °C for 0, 2, 4, 6, 8, 10, 12 and 24 h, concentration of compounds in samples were detected by using LC-MS.

Microsome stability assay. Compound **11l** or **11l-NC** (1 μM) was incubated with 0.5 mg/mL human, rat and mouse liver microsomes, respectively. NADPH was maintained at 1 mM in 1000 μL of reaction volume. The reaction was terminated by the addition of acetonitrile after 0, 5, 15, 30, 45, 60 and 90 min incubation, respectively. Samples were centrifuged for 15 min at 6000 rpm, and the compound concentration in supernatant was analyze by using high performance liquid chromatography with tandem mass spectrometric detection (LC-MS, 5500QTRAP system, Applied Biosystems).

***In vivo* oral bioavailability assay.** Oral bioavailability of compound **11l** and **11l-NC** were conducted in male Sprague-Dawley (SD) rats (Chinese Academy of Medical Science, Beijing, China). Briefly, catheters were surgically placed into the jugular veins of rats to collect serial blood samples. The rats were administered a single dose of **11l** and **11l-NC** at 25 mg/kg by oral gavage or 5 mg/kg by intravenous tail vein injection after fasting overnight, respectively. Blood was collected at the indicated time and centrifuged immediately to isolate plasma. The plasma concentration of compounds was determined by LC-MS (5500QTRAP system, Applied Biosystems). Noncompartmental pharmacokinetic parameters were fitted using DAS software (Enterprise, version2.0, Mathematical Pharmacology Professional Committee of China).

***In Vivo* Xenograft Studies.** The female NOD-SCID mice were purchased from Beijing HFK Bioscience Co. Ltd. (Beijing, China). Raji cells were harvested during the exponential-growth phase and washed twice with serum-free medium. Mice (6-7 weeks

old) were subcutaneously injected with 1×10^7 Raji cells, which were suspended in 0.05 mL of serum and antibiotic free growth medium, and 0.05 ml basement membrane matrix. When tumor volume reached to 100-200 mm^3, mice were randomly divided into five groups, including compound **11l** (30 mg/kg/d, suspended in 5% (v/v) NMP plus 95% (v/v) PEG400), **11l-NC** (40 or 80 mg/kg/d), BRQ (10 mg/kg/d, suspended in 30% (v/v) PEG300 plus 70% sodium chloride injection) (n = 6 for each group). The body weight and tumor volume were measured every 3 days. The volume was calculated as follows: tumor size = ab^2/2 (a, long diameter; b, short diameter). Percentage of tumor growth inhibition (TGI) was calculated as $100 \times \{1-[(\text{treated final day} - \text{treated initial day})/(\text{control final day} - \text{control initial day})]\}$.).The tissues of heart, liver, spleen, lung, and kidney were stained with H&E. Finally, images were acquired on an Olympus digital camera attached to a light microscope. The animal studies were conducted under the approval of the Experimental Animal Management Committee of Sichuan University.

Acute toxicity assay. The female and male BALB/c mice (6-8 weeks old) were obtained from Chinese Academy of Medical Science (Beijing, China) and used in present study. To investigate potential toxicity of compound **11l** and **11l-NC**, mice were orally administrated compound **11l** and **11l-NC** at the highest dose of 400 mg/kg and 800 mg/kg within 24 h, respectively. Rats were observed continuously for relevant indices such as body weight loss, diarrhea, anorexia, and skin ulcer or toxic death. On the 14th day, rats were euthanized after blood collection for blood chemistry analysis.

ASSOCIATED CONTENT

Supporting Information

X-ray diffraction data, particle size and PDI data, lipophilicity and solubility data, physiological stability data, metabolic stability data, in vivo anti-lymphoma assays of compound **11l** and H&E staining, IC$_{50}$ values of compounds against hDHODH, copies of NMR spectra, HPLC purity analysis for compound **11k, 11l, 11r** and **11s** (PDF)

molecular formula strings and associated biological data (CSV)

Accession Codes

Coordinates and structure factors for structures of compound **11k, 11l, 11s and 11r** have been deposited in the Protein Data Bank with the accession code of 6LP7, 6JME, 6LP6 and 6LP8. Authors will release the atomic coordinates and experimental data upon article publication.

AUTHOR INFORMATION

Corresponding Author

[a](Y.Z.) Phone : +86 28-85502796; E-mail : zhaoyinglan@scu.edu.cn.

[a](Y.L.) Phone : +86 28-85502796; E-mail : luo_youfu@scu.edu.cn.

Author Contributions

[#]Z.Z., X.L, X.Q., T.Z. contributed equally to this work.

Notes

The authors declare no competing financial interest.

ACKNOWLEDGEMENTS

ABBREVIATIONS

*h*DHODH, human dihydroorotate dehydrogenase; DHO, dihydroorotate; ORO, Orotate; CoQ, ubiquinone; FMN, flavin mononucleotide; SAR, structure activity relationship; LipE, lipophilic ligand efficiency.

REFERENCES

1. Mclean, J. E.; Neidhardt, E. A.; Grossman, T. H.; Hedstrom, L. Multiple inhibitor analysis of the brequinar and leflunomide binding sites on human dihydroorotate dehydrogenase. *Biochemistry* **2001**, *40*, 2194-2200.

2. Jones, M. E. Pyrimidine nucleotide biosynthesis in animals: genes,enzymes; regulation of UMP biosynthesis. *Annu. Rev. Biochem.* **1980**, *49*, 253-279.

3. Hines, V.; Johnston, M. Analysis of the kinetic mechanism of thebovine liver mitochondrial dihydroorotate dehydrogenase. *Biochemistry* **1989**, *28*, 1222-1226.

4. Sykes, D. B.; Kfoury, Y. S.; Mercier, F. E.; Wawer, M. J.; Law, J. M.; Haynes, M. K.; Lewis, T. A.; Schajnovitz, A.; Jain, E.; Lee, D.; Meyer, H.; Pierce, K.A.; Tolliday, N. J.; Waller, A.; Ferrara, S. J.; Eheim, A. L.; Stoeckigt, D.; Maxcy, K. L.; Cobert, J. M.; Bachand, J.; Szekely, B. A.; Mukherjee, S.; Sklar, L. A.; Kotz, J. D.; Clish, C. B.; Sadreyev, R. I.; Clemons, P. A.; Janzer, A.; Schreiber, S. L.; Scadden, D.T. Inhibition of dihydroorotate dehydrogenase overcomes differentiation blockade in acute myeloid leukemia. *Cell* **2016**, *1*, 171-186.

5. Lewis, T. A.; Sykes, D. B.; Law, J. M.; Munoz, B.; Rustiguel, J. K.; Nonato, M. C.; Scadden, D. T.; Schreiber, S. L. Development of ML390: a human DHODH inhibitor that induces differentiation in acute myeloid leukemia. *ACS Med. Chem. Lett.* **2016**, *7*, 1112-1117.

6. Mathur, D.; Stratikopoulos, E.; Ozturk, S.; Steinbach, N.; Pegno, S.; Schoenfeld, S.; Yong, R.; Murty, V. V,; Asara, J. M.; Cantley, L. C. PTEN regulates glutamine flux to pyrimidine synthesis and sensitivity to dihydroorotate dehydrogenase inhibition. *Cancer Discov.* **2017**, *7*, 380-390.

7. Koundinya, M.; Sudhalter, J.; Courjaud, A.; Lionne, B.; Touyer, G.; Bonnet, L.; Menguy, I.; Schreiber, I.; Perrault, C.; Vougier, S.; Benhamou, B.; Zhang, B.; He, T.; Gao, Q.; Gee, P.; Simard, D.; Castaldi, M. P.; Tomlinson, R.; Reiling, S.; Barrague, M.; Newcombe, R.; Cao, H.; Wang, Y.; Sun, F.; Murtie, J.; Munson, M.; Yang, E.; Harper, D.; Bouaboula, M.; Pollard, J.; Grepin, C.; Garcia-Echeverria, C.; Cheng, H.; Adrian, F.; Winter, C.; Licht, S.; Cornella-Taracido, I.; Arrebola, R.; Morris, A. Dependence on the pyrimidine biosynthetic enzyme DHODH is a synthetic lethal vulnerability in mutant kras-driven cancers. *Cell Chem. Biol.* **2018**, *25*, 705-717.

8. Ladds, M.; Vanleeuwen, I. M. M.; Drummond, C. J.; Chu, S.; Healy, A. R.; Popova, G.; Pastor Fernandez, A.; Mollick, T.; Darekar, S.; Sedimbi, S. K.; Nekulova, M.; Sachweh, M. C. C.; Campbell, J.; Higgins, M.; Tuck, C.; Popa, M.; Safont, M. M.;

Gelebart, P.; Fandalyuk, Z.; Thompson, A. M.; Svensson, R.; Gustavsson, A. L.; Johansson, L.; Farnegardh, K.; Yngve, U.; Saleh, A.; Haraldsson, M.; D'Hollander, A. C. A.; Franco, M.; Zhao, Y.; Hakansson, M.; Walse, B.; Larsson, K.; Peat, E. M.; Pelechano, V.; Lunec, J.; Vojtesek, B.; Carmena, M.; Earnshaw, W. C.; McCarthy, A. R.; Westwood, N. J.; Arsenian-Henriksson, M.; Lane, D. P.; Bhatia, R.; McCormack, E.; Lain, S. A DHODH inhibitor increases p53 synthesis and enhances tumor cell killing by p53 degradation blockage. *Nat. Commun.* **2018**, *9*, 1107-1120.

9. Sun, C.; Wang, L.; Huang, S.; Heynen, G. J.; Prahallad, A.; Robert, C.; Haanen, J.; Blank, C.; Wesseling, J.; Willems, S. M.; Zecchin, D.; Hobor, S.; Bajpe, P. K.; Lieftink, C.; Mateus, C.; Vagner, S.; Grernrum, W.; Hofland, I.; Schlicker, A.; Wessels, L. F.; Beijersbergen, R. L.; Bardelli, A.; Di Nicolantonio, F.; Eggermont, A. M.; Bernards, R. Reversible and adaptive resistance to BRAF(V600E) inhibition in melanoma. *Nature* **2014**, *508*, 118-122.

10. Mohamad, F. A. K.; Choudhary, B.; Hosahalli, S.; Kavitha, N.; Shatrah, O. Dihydroorotate dehydrogenase (DHODH) inhibitors affect ATP depletion, endogenous ROS and mediate S-phase arrest in breast cancer cells. *Biochimie*. **2017**, *135*, 154-163.

11. Brown, K. K.; Spinelli, J. B.; Asara, J. M.; Toker, A. Adaptive reprogramming of *de novo* pyrimidine synthesis is a metabolic vulnerability in triple-negative breast cancer. *Cancer Discov.* **2017**, *7*, 391-399.

12. Breedveld, F. C.; Dayer, J. M. Leflunomide: mode of action in the treatment of rheumatoid arthritis. *Ann. Rheum. Dis.* **2000**, *59*, 841-849.

13. Herrmann, M. L.; Schleyerbach, R.; Kirschbaum, B. J. Leflunomide: an immunomodulatory drug for the treatment of rheumatoid arthritis and other autoimmune diseases. *Immunopharmacology*. **2000**, *47*, 273-289.

14. Leflunomide + vemurafenib in V600 mutant met melanoma. *ClinicalTrials.gov*; U.S. national institutes of health: Bethesda. MD, June 5, 2012; https://clinicaltrials.gov/show/NCT01611675 (accessed Mar 11, 2020).

15. A phase I/II trial of leflunomide in previously treated metastatic triple negative cancers. *ClinicalTrials.gov*; U.S. national institutes of health: Charles shapiro, MD, October 17, 2018; https://clinicaltrials.gov/show/NCT03709446 (accessed Mar

11,2020).

16. Natale, R.; Wheeler, R,; Moore, M,; Dallaire, B,; Lynch, W,; Carlson, R. Grillo-Lopez, A.; Gyves, J. Multicenter phase II trial of brequinar sodium in patients with advanced melanoma. *Ann. Oncol.* **1992**, *3*, 659-660.

17. Schwartsmann, G.; Dodion, P.; Vermorken, J. B.; W, W.; Huinink, B.T.; Winograd, B. Gall, H.; Simonetti, G.; Van der Vijgh, W. J. F.; Van Hennik, M. B.; Crespeigne, N.; Pinedo, H. M. Phase I study of brequinar sodium (NSC 368390) in patients with solid malignancies. *Cancer Chemother. Pharmacol.* **1990**, *25*, 345-351.

18. Urba, S.; Doroshow. J.; Cripps, C.; Robert, F.; Velez-Garcia, E.; Dallaire, B.; Adams, D.; Carlson, R.; Grillo-Lopez, A.; Gyves, J. Multicenter phase II trial of brequinar sodium in patients with advanced squamous-cell carcinoma of the head and neck. *Cancer Chemother. Pharmacol.* **1992**, *31*, 167-169.

19. Moore, M.; Maroun, J.; Robert, F.; Natale, R.; Neidhart, J.; Dallaire, B.; Sisk, R.; Gyves, J. Multicenter phase II study of brequinar sodium in patients with advanced gastrointestinal cancer. *Invest. New Drugs* **1993**, *11*, 61-65.

20. Maroun, J.; Ruckdeschel, J.; Natale, R.; Morgan, R.; Dallaire, B.; Sisk, R.; Sisk, R.; Gyves, J. Multicenter phase II study of brequinar sodium in patients with advanced lung cancer. *Cancer Chemother. Pharmacol.* **1993**, *32,* 64-66.

21. Cody, R.; Stewart, D.; DeForni, M.; Moore, M.; Dallaire, B.; Azarnia, N.; Gyves, J. Multicenter phase II study of brequinar sodium in patients with advanced breast cancer. *Am. J. Clin. Oncol.* **1993**, *16*, 526-528.

22. Munier-Lehmann, H.; Vidalain, P. O.; Tangy, F.; Janin, Y. L. On dihydroorotate dehydrogenases and their inhibitors and uses. *J. Med. Chem.* **2013**, *56*, 3148-3167.

23. Lolli, M. L.; Sainas, S.; Pippione, A. C.; Giorgis, M.; Boschi, D.; Dosio, F. Use of human dihydroorotate dehydrogenase (hDHODH) Inhibitors in autoimmune diseases and new Perspectives in cancer therapy. *Recent Pat. Anti-Canc.* **2018**, *13*, 86-105.

24. Madak, J. T.; Cuthbertson, C. R.; Miyata, Y.; Tamura, S.; Petrunak, E. M.; Stuckey, J. A.; Han, Y.; He, M.; Sun, D.; Showalter, H. D.; Neamati, N. Design, synthesis, and biological evaluation of 4-quinoline carboxylic acids as inhibitors of dihydroorotate dehydrogenase. *J. Med. Chem.* **2018**, *61*, 5162-5186.

25. Sainas, S.; Pippione, A. C.; Lupino, E.; Giorgis, M.; Circosta, P.; Gaidano, V.; Goyal, P.; Bonanni, D.; Rolando, B.; Cignetti, A.; Ducime, A.; Andersson, M.; Jarva, M.; Friemann, R.; Piccinini, M.; Ramondetti, C.; Buccinna, B.; Al-Karadaghi, S.; Boschi, D.; Saglio, G.; Lolli, M. L. Targeting myeloid differentiation using potent 2-hydroxypyrazolo[1,5- a]pyridine scaffold-based human dihydroorotate dehydrogenase inhibitors. *J. Med. Chem*. **2018**, *61*, 6034-6055.

26. A phase 1, 2-part study to evaluate the safety, tolerability and pharmacokinetics of multiple doses of ASLAN003 in healthy elderly subjects. *ClinicalTrials.gov*; U.S. national institutes of health: Aslan Pharmaceuticals, January 21, 2014; https://clinicaltrials.gov/show/NCT02342652 (accessed Mar 11, 2020).

27. A study to investigate BAY2402234, a dihydroorotatedehydrogenase (DHODH) inhibitor, in myeloid Malignancies. ClinicalTrials.gov; U.S. national institutes of health: Bayer. January 19, 2018; https://clinicaltrials.gov/show/NCT03404726 (accessed Mar 11, 2020).

28. A study of AG-636 in the treatment of subjects with advanced lymphoma. *ClinicalTrials.gov*; U.S. national institutes of health: Agios Pharmaceuticals, February 8, 2019; https://clinicaltrials.gov/show/NCT03834584 (accessed Mar 11, 2020).

29. Christian, S.; Merz, C.; Evans, L.; Gradl, S.; Seidel, H.; Friberg, A.; Eheim, A.; Lejeune, P.; Brzezinka, K.; Zimmermann, K.; Ferrara, S.; Meyer, H.; Lesche, R.; Stoeckigt, D.; Bauser, M.; Haegebarth, A.; Sykes, D. B.; Scadden, D.T.; Losman, J. A.; Janzer, A. The novel dihydroorotate dehydrogenase (DHODH) inhibitor BAY 2402234 triggers differentiation and is effective in the treatment of myeloid malignancies. *Leukemia* **2019**, *33*, 2403-2415.

30. Fang, J. X.; Uchiumi, T.; Yagi, M.; Matsumoto, S.; Amamoto, R.; Takazaki, S.; Yamaza, H.; Nonak, K.; Kang, D. C. Dihydro-orotate dehydrogenase is physically associated with the respiratory complex and its loss leads to mitochondrial dysfunction. *Biosci. Rep.* **2013**, *33,* 25-33.

31. Trachootham, D.; Alexandre, J.; Huang, P. Targeting cancer cells by ROS-mediated mechanisms:a radical therapeutic approach. *Nat. Rev. Drug Discov.* **2009**, *8*, 579-591.

32. Pelicano, H.; Carney, D.; Huang, P.ROS stress in cancer cells and therapeutic implications. *Drug Resist. Updat.* **2004**, *7*, 97-110.

33. Froeling, FEM.; Swamynathan, M.M.; Deschênes, A.; Chio, II.C.; Brosnan, E.; Yao, M. A.; Alagesan, P.; Lucito, M.; Li, J.; Chang, A.Y.; Trotman, L. C.; Belleau, P.; Park, Y.; Rogoff, H. A.; Watson, J. D.; Tuveson, D. A. Bioactivation of napabucasin triggers reactive oxygen species–mediated cancer cell death. *Clin. Cancer Res.* **2019**, *25*, 7162-7174.

34. Damiani, R. M.; Moura, D. J.; Viau, C. M.; Caceres, R. A.; Henriques, J. A. P.; Saffi, J. Pathways of cardiac toxicity: comparison between chemotherapeutic drugs doxorubicin and mitoxantrone. *Arch. Toxicol.* **2016**, *90,* 2063-2076.

35. Serrano, J.; Palmeira, C.M.; Kuehl, D. W.; Wallace, K. B. Cardioselective and cumulative oxidation of mitochondrial DNA following subchronic doxorubicin administration. *Biochim. Biophys. Acta.* **1999**, *1411*, 201-205.

36.Hong, Y.; Sengupta, S.; Hur, W.; Sim, T. Identification of novel ROS inducers: quinone derivatives tethered to long hydrocarbon chains. *J. Med. Chem.* **2015**, *58*, 3739-3750.

37. Hubbard, J. M.; Grothey, A. Napabucasin: an update on the first-in-class cancer stemness inhibitor. *Drugs* **2017**, *77*, 1091-1103.

38. Knecht, W.; Henseling, J.; Loffler, M. Kinetics of inhibition of human and rat dihydroorotate dehydrogenase by atovaquone, lawsone derivatives, brequinar sodium and polyporic acid. *Chem-Biol. Interact.* **2000**, *124*, 61-76.

Seymour, K. K.; Lyons, S. D.; Phillips, L.; Rieckmann, K. H.; Christopherson, R. I. Cytotoxic effects of inhibitors of de novo pyrimidine biosynthesis upon Plasmodium falciparum. *Biochemistry* **1994**, *33*, 5268-5274

40. Tao, C.Z.; Cui, X.; Li, J.; Liu, A.X.; Liu, L.; Guo, Q.X. Copper-catalyzed synthesis of aryl azides and 1-aryl-1,2,3-triazoles from boronic acids. *Tetrahedron Lett.* **2007**, *48*, 3525-3529.

41. Singh, H.; Khanna, G.; Khurana, J. M. DBU catalyzed metal free synthesis of fused 1,2,3-triazoles through [3+2] cycloaddition of aryl azides with activated cyclic C–H acids. *Tetrahedron Lett.* **2016**, *57*, 3075-3080.

42. Bebensee, F.; Bombis, C.; Vadapoo, S. R.; Cramer, J. R.; Besenbacher, F.; Gothelf, K. V.; Linderoth, T. R. On-surface azide-alkyne cycloaddition on Cu(111): does it "click" in ultrahigh vacuum. *J. Am. Chem. Soc.* **2013**, *135*, 2136-2139.

43. Hopkins, A. L.; Keseru, G. M.; Leeson, P. D.; Rees, D. C.; Reynolds, C. H. The role of ligand efficiency metrics in drug discovery. *Nat. Rev. Drug Discov.* **2014**, *13*, 105-121.

44. Vyas, V. K.; Ghate, M. Recent developments in the medicinal chemistry and therapeutic potential of dihydroorotate dehydrogenase (DHODH) Inhibitors. *Mini-Rev. Med. Chem.* **2011**, *11*, 1039-1055.

45. Liu, S.; Neidhardt, E. A.; Grossman, T. H.; Ocain, T.; Clardy, J. Structures of human dihydroorotate dehydrogenase in complex with antiproliferative agents. *Structure* **2000**, *8*, 25-33.

46. Zhu, J.; Han, L.; Diao, Y.; Ren, X.; Xu, M.; Xu, L.; Li, S.; Li, Q.; Dong, D.; Huang, J.; Liu, X.; Zhao, Z.; Wang, R.; Zhu, L.; Xu, Y.; Qian, X.; Li, H. Design, synthesis, X-ray crystallographic analysis, and biological evaluation of thiazole derivatives as potent and selective inhibitors of human dihydroorotate dehydrogenase. *J. Med. Chem.* **2015**, *58*, 1123-1139.

47. Baumgartner, R.; Walloschek, M.; Kralik, M.; Gotschlich, A.; Tasler, S.; Mies, J.; Leban, J. Dual binding mode of a novel series of DHODH Inhibitors. *J. Med. Chem.* **2006**, *49*, 1239-1247.

48. Walse, B.; Dufe, V. T.; Svensson, B.; Fritzson, I.; Dahlberg, L.; Khairoullina, A.; Wellmar, U.; Ai, K. S. The structures of human dihydroorotate dehydrogenase with and without inhibitor reveal conformational flexibility in the inhibitor and substrate binding sites. *Biochemistry* **2008**, *47*, 8929–8936.

49. Yustein, J. T.; Dang, C. V. Biology and treatment of Burkitt's lymphoma. *Curr. Opin. Hematol.* **2007**, *14*, 375–381.

50. Koundinya, M.; Sudhalter, J.; Courjaud, A.; Lionne, B.; Touyer, G.; Bonnet, L.; Menguy, I.; Schreiber, I.; Perrault, C.;Vougier, S.; Benhamou, B.; Zhang, B.; He, T.; Gao, Q.; Gee, P.; Simard, D.; Castaldi, M. P.; Tomlinson，R.; Reiling, S.; Barrague, M.; Newcombe, R.; Cao, H.; Cao, H.; Sun, F.; Murtie, J.; Munson, M.; Yang,

E.; Harper, D.; Bouaboula, M.; Pollard, J.; Grepin, C.; Garcia-Echeverria, C.; Cheng, H.; Adrian, F.; Winter, C.; Licht, S.; Cornella-Taracido, I.; Arrebola, R.; Morris, A. Dependence on the pyrimidine biosynthetic enzyme DHODH is a synthetic lethal vulnerability in mutant KRAS-driven cancers. *Cell Chem. Biol.* **2018**, *25*, 705-717.

51. Noe, D. A.; Rowinsky, E. K.; Shen, H. S.; Clarke, B. V.; Grochow, L. B.; McGuire, W. B.; Hantel, A.; Adams, D. B.; Abeloff, M. D.; Ettinger, D. S.; Donehower, R. C. Phase I and pharmacokinetic study of brequinar sodium (NSC 368390). *Cancer Res.* **1990**, *50*, 4595-4599.

52. Dorasamy, M. S.; Ab, A.; Nellore, K.; Wong, P. F. Synergistic inhibition of melanoma xenografts by Brequinar sodium and Doxorubicin. *Biomed. Pharmacother*. **2019**, *110*, 29-36.

53. Merrill, J.; Hanak, S.; Pu, S. F.; Liang, J.; Dang, C.; Iglesias, B. D.; Harvey, B.; Zhu, B.; McMonagle, S. K. Teriflunomide reduces behavioral, electrophysiological, and histopathological deficits in the dark agouti rat model of experimental autoimmune encephalomyelitis. *J. Neurol.* **2009**, *256*, 89-103.

54. Matthew, D.; Timo, H.; Glenn, A. M.; Colin, W. G. F.; Mark, R. P.; Johnson, A. P. Structure-based design, synthesis, and characterization of inhibitors of human and *plasmodium falciparum* dihydroorotate dehydrogenases. *J. Med. Chem*. **2009**, *52*, 2683-2693.

55. Baldwin, J.; Farajallah, A. M.; Malmquist, N. A.; Rathod, P. K.; Phillips, M. A. Malarial dihydroorotate dehydrogenase. Substrate and inhibitor specificity. *J. Biol. Chem.* **2002**, *277*, 41827-41834.

56. Hurt, D. E.; Widom, J.; Clardy. J. Structure of plasmodium falciparum dihydroorotate dehydrogenase with a bound inhibitor. *Acta Crystallogr*., *D: Biol. Crystallogr.* **2006**, *62*, 312-323.

57. Minor, W.; Cymborowski, M.; Otwinowski, Z.; Chruszc, M. HKL-3000: The integration of data reduction and structure solution - From diffraction images to an initial model in minutes. *Acta Crystallogr*., *Sect. D: Biol. Crystallogr.* **2006**, *62*, 859-866.

58. Adams, P. D.; Afonine, P. V.; Bunkoczi. G.; Chen, V. B.; Davis, I. W.; Echols,

N.; Headd, J. J.; Hung, L. W.; Kapral, G. J.; Grosse-Kunstleve, R. W.; McCoy, A. J.; Moriarty, N. W.; Oeffner, R.; Read, R. J.; Richardson, D. C.; Richardson, J. S.; Terwilliger, T. C.; Zwart, P. H. PHENIX: A comprehensive python-based system for macromolecular structure solution. *Acta Crystallogr.*, *Sect. D: Biol. Crystallogr.* **2010**, *66*, 213-221.

59. Emsley, P.; Cowtan, K. Coot: Model-building tools for molecular graphics. *Acta Crystallogr.*, *Sect. D: Biol.* Crystallogr. **2004**, *60*, 2126-2132.

60. Chen,V. B.; Arendall, W. B.; Headd. J. J.; Keedy, D. A.; Immormino, R. M.; Kapral, G. J.; Murray, L. W.; Richardson, J. S.; Richardson, D. C. MolProbity: All-atom structure validation for macromolecular crystallography. *Acta Crystallogr., Sect. D: Biol. Crystallogr.* **2010**, *66*, 12-21.

1
2
3
4
5
6
7
8
9
10
11
12
13
14
15
16
17
18
19
20
21
22
23
24
25
26
27
28
29
30
31
32
33
34
35
36
37
38
39
40
41
42
43
44
45
46
47
48
49
50
51
52
53
54
55
56
57
58
59
60

TABLE OF CONTENTS GRAPHIC

11l

IC_{50} = 4.5 nM for hDHODH
IC_{50} = 0.02 μM for A375
IC_{50} = 0.29 μM for HCT116
IC_{50} = 0.16 μM for Raji
IC_{50} = 0.11 μM for K562
IC_{50} = 0.99 μM for Nalmawa

MTD of 11-NC = 800 mg/kg